ACS Partner Journal

CHEMICAL & BIOMEDICAL IMAGING

pubs.acs.org/ChemBioImaging

Article

Recombinant–Chemosynthetic Biosensors for Probing Cell Surface Signaling of Red Blood Cells and Other Cells

Sithurandi Ubeysinghe,[§] Chloe O. Sebilleau,[§] Waruna Thotamune,[§] Chathuri Rajarathna, Samuel Azibere, Mithila Tennakoon, John L. Payton, Randy S. Sprague, R. Scott Martin, Steven J. Sucheck,* and Ajith Karunarathne*

Cite This: *Chem. Biomed. Imaging* 2025, 3, 95–110

Read Online

ACCESS | Metrics & More | Article Recommendations | Supporting Information

ABSTRACT: The complex signaling mechanisms in red blood cells (RBCs) enable them to adapt to physiological stresses such as exposure to low O_2 levels, metabolic demands, oxidative stress, and shear stress. Since Ca^{2+} is a crucial determinant of RBC fate, various ion channels, pumps, and exchangers regulate the delicate balance of Ca^{2+} influx and efflux in RBCs. Elevated intracellular Ca^{2+} can activate processes such as membrane phospholipid scrambling and alter RBC deformability, which is essential for effective capillary transit. However, the dynamic information about Ca^{2+} regulation in RBCs is limited. Although static mapping and bioanalytical methods have been utilized, the absence of a nucleus and the presence of hemoglobin create challenges for real-time probing of RBC signaling, necessitating innovative approaches. This work introduces a synthetic chemistry–recombinant protein-based strategy to assemble sensors at genetically intact healthy human RBC surfaces for measuring dynamic signaling. Using this approach, we measured autocrine regulation of RBC Ca^{2+} influx in response to low O_2 tension-induced ATP release. The study also explores the utilization of synthetic glycosylphosphatidylinositol (GPI) anchor mimics and sortagging for targeting sensors to the surfaces of primary as well as immortalized cells. This demonstrated the wide applicability of this approach to probe dynamic signaling in intact cells.

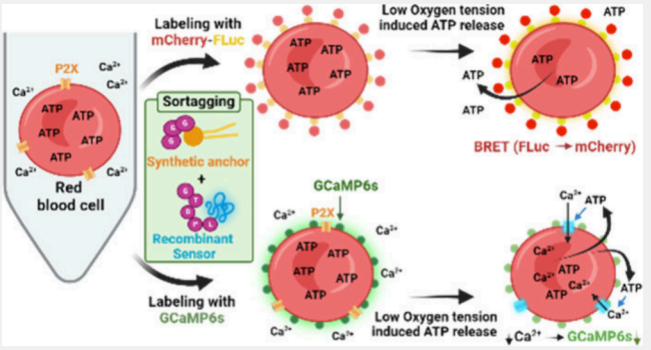

KEYWORDS: *Ca^{2+}, GCaMP6s, P2X, GPI anchor mimics, TIRF imaging, RBCs, sortase A, cellular signaling*

1. INTRODUCTION

Ca^{2+} is a major secondary messenger that controls crucial and deterministic cellular functions, and thus, its concentrations at various subcellular compartments are tightly regulated.[1,2] For instance, Ca^{2+} controls signaling underlying muscle contractility, blood clotting, bone mineralization, cell motility, and apoptosis.[3−6] Dysregulation of Ca^{2+} availability, both the deficiency and overloading, can bring about destructive consequences to cells.[7] Therefore, multicellular organisms monitor and adjust cell exterior Ca^{2+} concentrations in body fluids (i.e., blood, cerebrospinal fluid, and lymph) to maintain a stable cellular environment.[8] Moreover, multiple cellular mechanisms are employed to buffer, sequester, accumulate, and mobilize Ca^{2+} in cells to maintain cell interior Ca^{2+} concentrations within strict limits. In early studies, the changes in extracellular Ca^{2+} concentration in the rat cerebellum were measured using double-barreled Ca^{2+}-selective micropipettes.[9] In anesthetized Wistar rats, *in situ* microdialysis techniques have been used to monitor extracellular Ca^{2+} concentration in the subepithelial spaces of the intestine.[10] Ca^{2+}-sensitive metallochromic indicators (antipyrylazo III and tetramethylmurexide) have also been used to detect extracellular Ca^{2+} dynamics in beating hearts.[11] The droplet technique based on the activity of the plasma membrane Ca^{2+}-ATPase was exploited to measure extracellular Ca^{2+} changes.[11] Ca^{2+}-Green-C-18, the fluorophore-conjugated with a lipid derivative, has been used to record Ca^{2+} fluctuations inside the T-tubules.[11] Additionally, Ca^{2+}-sensitive probes conjugated to a hydrophobic tail have been used to cross the external leaflet of the cell membrane and directly measure extracellular Ca^{2+} levels.[11] In smooth muscle cells, the Ca^{2+}-sensitive indicator Fura-C18 was employed to measure extracellular Ca^{2+} changes near the plasma membrane. In contrast to the success of intracellular Ca^{2+} measurements, detecting Ca^{2+} fluctuations on the cell surface presents significant challenges.

Received: September 19, 2024
Revised: December 21, 2024
Accepted: December 24, 2024
Published: January 3, 2025

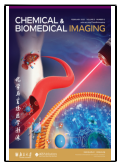

Scheme 1. Strategy for the Synthesis of Compound 1 and H_2N-GGGYC-Maleimide-PEG-DOPE (Compound 2)

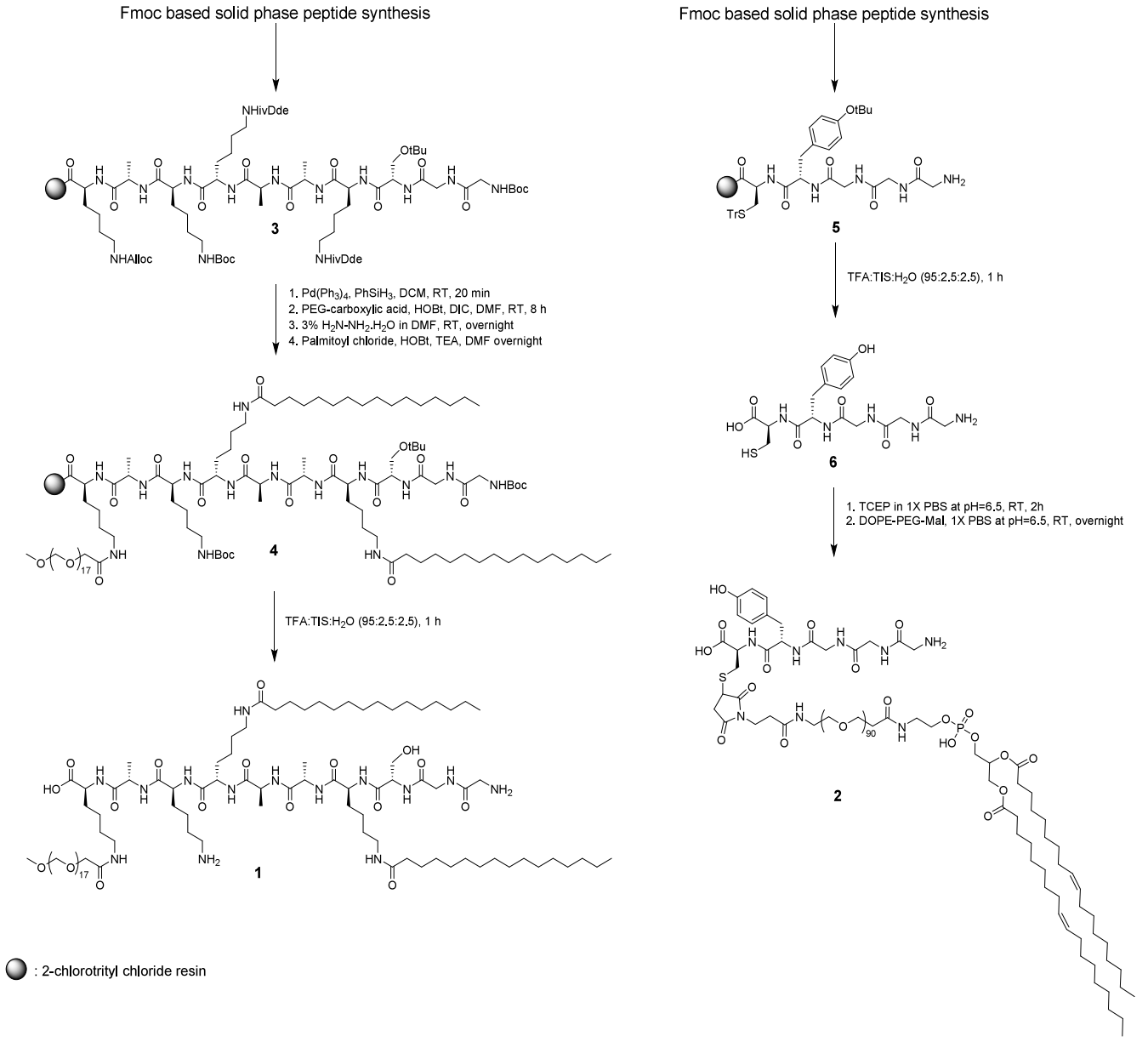

Red blood cells (RBCs) are essential components of the circulatory system. RBCs lack the nucleus and organelles, maximizing space for hemoglobin and sustaining a high O_2-carrying capacity. RBCs have complex signaling mechanisms that operate various protein kinases and phosphatases. This allows them to quickly adapt to multiple physiological stresses such as exposure to low O_2 levels, metabolic demands, oxidative stress, and shear stress.[12−17] Furthermore, mechanical stress and changes in O_2 levels activate ion transporters and specific phosphorylation events, which affect cell volume and membrane properties.[12] Various ion channels, pumps, and exchangers regulate intracellular Ca^{2+} levels in RBCs since the disruptions in Ca^{2+} homeostasis can lead to altered RBC function and even hemolysis.[18] In RBCs, elevated intracellular Ca^{2+} can activate several processes, including the scrambling of membrane phospholipids, marking the cell for clearance by the spleen.[18] Additionally, increased Ca^{2+} influences RBC deformability and rheology in microvasculature.[19] Understanding the dynamic behavior of these signaling pathways is crucial to providing potential therapeutic strategies for hemoglobinopathies and channelopathies, emphasizing the importance of targeting signaling elements to improve RBC function in various pathological conditions.

While cell-destructive approaches such as proteomics and biochemical analysis of involved proteins have been used to generate static maps of signaling,[20−22] dynamic bioanalytical methods including microflow analysis,[23] microfluidic devices,[24−28] 3D vasculature mimics[29,30] and capillary electrophoresis[31] have been used to examine a handful of chemical messengers released by physically and pharmacologically perturbed RBCs. Considering the vital role of RBCs in a plethora of critical pathophysiological functions in humans and other organisms, innovative approaches that can circumvent the above challenges are needed. However, the dynamic information about Ca^{2+} regulation in RBCs is limited since regular Ca^{2+} imaging in RBCs is challenging due to the unique characteristics of RBCs compared to the other cell types. For instance, the lack of a nucleus and organelles in RBCs[32] limits

https://doi.org/10.1021/cbmi.4c00067
Chem. Biomed. Imaging 2025, 3, 95−110

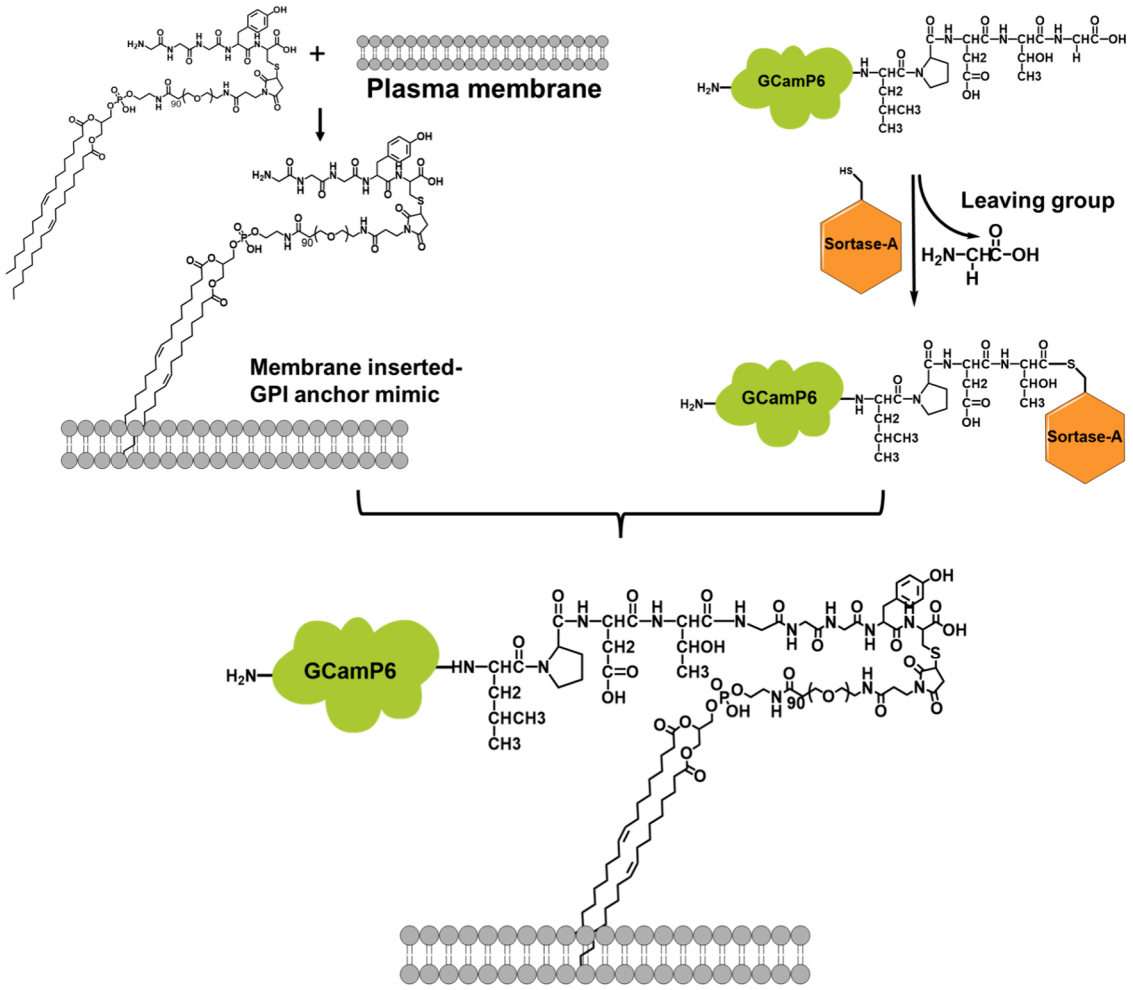

Figure 1. Schematic representation of the sortase A reaction between the membrane-anchored H_2N-GGGYC-Maleimide-PEG-DOPE and purified GCaMP6s-LPDTG.

the application of genetic manipulation techniques and conventional signaling pathway analysis. Additionally, technical limitations due to hemoglobin interference prevent the use of optical methods such as fluorescence.

In this work, we adapted a synthetic chemistry−recombinant protein-based strategy that can assemble different sensors at genetically intact cell surfaces, especially the surface of healthy human RBCs, to measure dynamic signaling. Since the regulation of Ca^{2+} plays a key role in RBC pathophysiology, we devised a novel strategy to measure autocrine regulation of RBC Ca^{2+} influx on low O_2 tension-induced ATP release. Cells use a specific mechanism to present over 150 proteins on the outer leaflet of the plasma membrane.[33] This mechanism involves a region at the carboxy-terminal of the proteins recognized by glycosylphosphatidylinositol (GPI) transamidase. This recognition allows the transamidase to create a covalent bond between a GPI glycolipid and the processed C-terminus of the protein.[34,35] Since the use of synthetic GPI anchors to target proteins to the cell surface is challenging, GPI anchor mimics have alternatively been employed. GPI anchors were mimicked using short lipidated peptides synthesized via solid-phase peptide synthesis (SPPS).[36] This approach requires fewer purification and synthetic steps while preserving targeting capabilities and offering a simpler alternative to more complex native-like GPI anchor mimics.[37] Our approach uses an efficient sortase A from *Staphylococcus aureus* to catalyze the ligation of a five amino acid substrate motif (LPXTG, X can be any amino acid) on the carboxy-terminal (Ct) of the protein and oligoglycine nucleophiles-tethered maleimide-based PEG-glycerolipid.[38] Although the use of sortase A-catalyzed modification of proteins with polyethylene glycol (PEG)-lipids has been employed to label and track cells,[39] our work introduces a novel approach for decorating the surfaces of genetically intact cells with various sensors for dynamic signaling events. In this study, we measure changes in RBC surface Ca^{2+} concentrations due to the influx through ATP-gated P2X channels using fluorescence and bioluminescence resonance energy transfer (BRET). Overall, our methodology holds significant potential to map dynamic signaling in primary cells, such as RBCs and neurons, which are difficult to probe using conventional techniques.

2. RESULTS AND DISCUSSION

2.1. Decoration of Cell Surfaces with Recombinant Protein-Based Sensors Using Sortase-Mediated Ligation (SML)

Our goal was to develop an optimized protocol for incorporating protein-based sensors at the cell surface without genetic modifications. Here, we selected GCaMP6s, which provides an ∼1.5-fold fluorescence increase upon Ca^{2+} binding as the Ca^{2+} sensor.[40] We first engineered the construct

https://doi.org/10.1021/cbmi.4c00067
Chem. Biomed. Imaging 2025, 3, 95−110

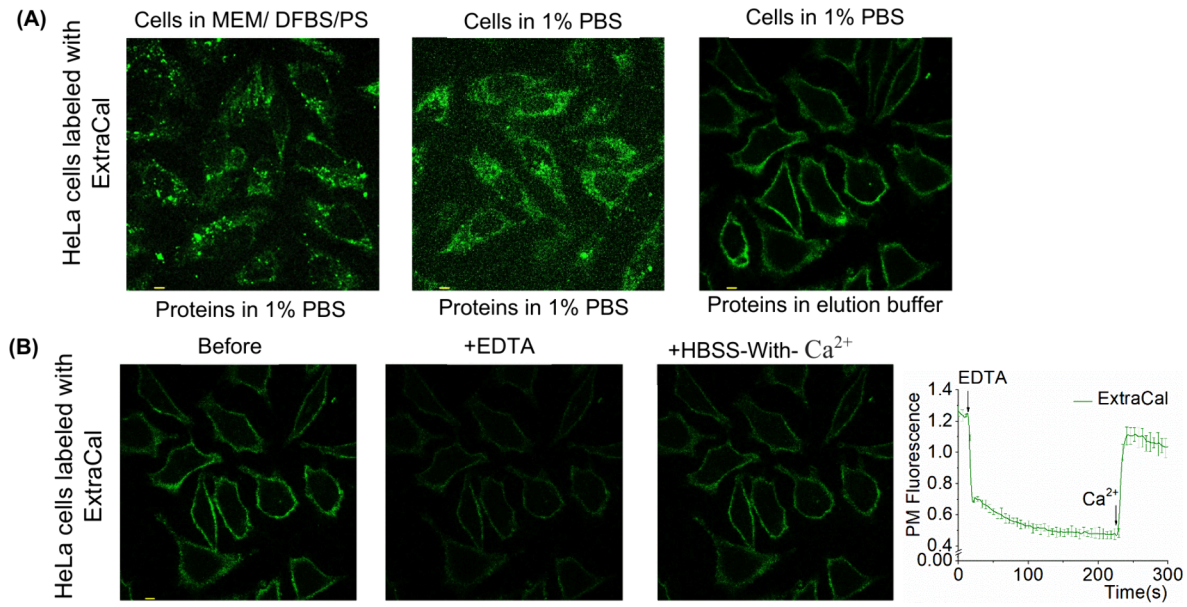

Figure 2. (A) Optimization of the cell labeling protocol in HeLa cells was performed under three different conditions: (left) cells are in MEM/DFBS/PS containing HeLa media and purified sortase A and GCaMP6s-LPDTG proteins are in 1% PBS; (middle) cells and purified sortase A and GCaMP6s-LPDTG proteins are in 1% PBS; (right) cells are in 1% PBS and purified sortase A and GCaMP6s-LPDTG proteins are in elution buffer. (B) HeLa cells labeled with ExtraCal showed a reduction in ExtraCal fluorescence upon EDTA addition and its fluorescence intensity was increased upon addition of HBSS containing Ca^{2+} (n = 25 cells from 3 repeats). The plot shows fluorescence change of ExtraCal upon EDTA followed by HBSS-With- Ca^{2+} addition over the course of 6 min. The error bars represent SD (standard error of standard deviation). Scale bar = 5 μm. EDTA, ethylenediaminetetraacetic acid; HBSS, Hanks' balanced salt solution.

encoding GCaMP6s with the LPDTG motif at the Ct in the pET32 bacterial expression vector and purified the recombinant protein using BL21 (DE3) competent cells. Subsequently, we synthesized compound **1** carrying diglycine nucleophile and compound **2** (H_2N-GGGYC-Maleimide-PEG-DOPE) with triglycine nucleophile as described in Materials and Methods (Scheme 1). The design of compound **1** was based on a previously reported GPI anchor mimic[36] that was modified to make the target more facile to prepare, thus easily accessible by less sophisticated synthetic laboratories. Since the commercially available wild-type sortase A was deemed inefficient in conjugating the protein with the triglycine nucleophile, we recombinantly purified a more efficient 5M (Penta mutant) sortase A variant.[41,42] The size and the purity of purified proteins were validated by SDS-PAGE (Figure S1A). Using HeLa cells as the sample cell type, we first optimized the labeling protocol using sortase A (5 M) (Figure 1). Though the initial labeling conditions 1 and 2 described in Materials and Methods resulted in internalization of the sensor (Figure 2A, left and middle), the optimized condition 3 exhibited efficient labeling of HeLa cells with GCaMP6s. The labeling mechanism involves sortase A binding to the LPDTG motif tethered to the sensor, cleaving between the *Thr* and *Gly* residues. This results in the formation of an acyl-enzyme intermediate complex between the sortase A active site *Cys* thiol and the carboxyl group of *Thr*. Finally, the intermediate is released following a nucleophilic attack by the amino group of the membrane-tethered triglycine nucleophile (Figure 1). The optimized protocol includes incubation of cells with H_2N-GGGYC-Maleimide-PEG-DOPE first to decorate the cell surface with the PEG-Maleimide lipid carrying the exposed triglycine, and subsequent incubation with the purified GCaMP6s-LPDTG protein in the presence of the improved sortase A. We named the cell surface anchored GCaMP6s "ExtraCal" henceforth. Figure 2A, right shows ExtraCal labeled HeLa cells using condition 3. We also employed condition 3 to label HeLa cells using compound **1** in place of compound **2**. These cells also exhibited efficient labeling (Figure S1B). Therefore, for all the subsequent labeling reactions, we used compound **2** (H_2N-GGGYC-Maleimide-PEG-DOPE).

Next, to examine whether ExtraCal senses extracellular Ca^{2+} changes, we treated ExtraCal-labeled HeLa cells in the MEM-based cell culture media (1 mL) with 200 μL of 2.5 μM EDTA (in PBS) making the final EDTA concentration in cells = 0.5 μM. Confocal time-lapse images of the sensor were collected during this process using 488 nm excitation and 521 nm emission. Upon EDTA addition, ExtraCal fluorescence on the cell membranes exhibited an ∼2-fold reduction (Figure 2B, +EDTA; cell images, plot, and Movie S1). However, ExtraCal fluorescence in HeLa cells treated only with 200 μL PBS remained unchanged (Figure S1C). Since MEM-basal media contains ∼1−2 mM Ca^{2+}, next we added 200 μL of HBSS-With-Ca^{2+} containing 1.3 mM $CaCl_2$ to the same cells. Cells exhibited near-complete recovery of the lost fluorescence incurred upon EDTA addition (Figure 2B, +HBSS-With-Ca^{2+}; cell images, plot, and Movie S1). This data collectively indicated that ExtraCal is able to sense dynamic changes in the extracellular Ca^{2+}. To examine the stability of the sensor's cell surface localization, we examined cells over 3 h, by capturing images at 30 min intervals. This showed that the localization remained intact, indicating the suitability of the labeling method for prolonged experiments (Figure S1D).

We also show that this labeling method can be successfully adopted for a wide variety of cell types. Cell types such as RAW264.7, AC16 (human cardiomyocytes), and differentiated 3T3L (adipocytes), and C2C12 (muscle cells) exhibited efficient labeling with ExtraCal (Figure S2). Additionally, primary cells including mouse primary fibroblasts, dorsal root

https://doi.org/10.1021/cbmi.4c00067
Chem. Biomed. Imaging 2025, 3, 95−110

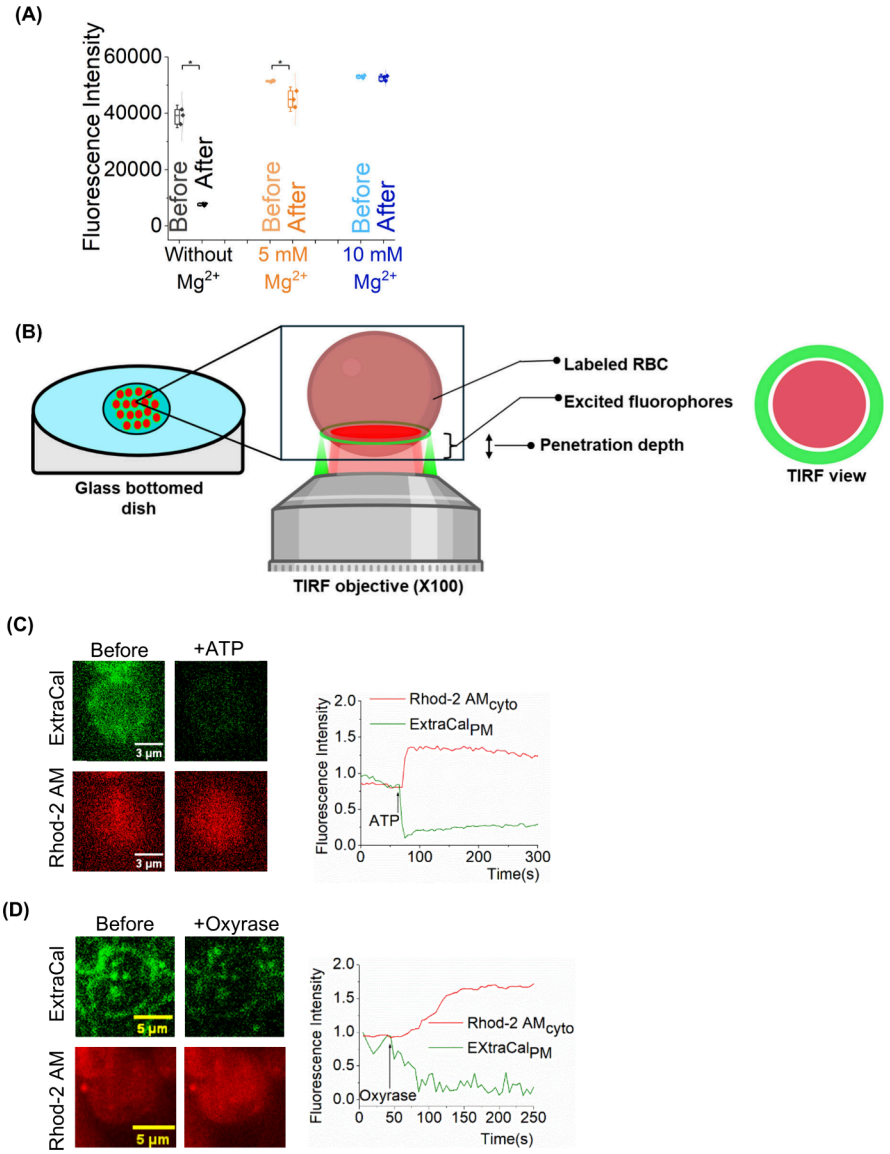

Figure 3. (A) ExtraCal exhibited negligible Ca^{2+} chelation upon ATP addition in the presence of 10 mM Mg^{2+}, compared to the samples containing 5 mM Mg^{2+} and no Mg^{2+}, in a Plate reader assay (n = 3 replicates). (B) Diagram depicting the TIRF imaging of Rhod 2-AM stained and ExtraCal labeled RBCs by controlling the penetration depth and the focal plane. (C) Rhod-2 AM stained and ExtraCal labeled healthy human RBCs exhibited a detectable ExtraCal fluorescence reduction and Rhod-2 AM fluorescence gain upon ATP addition, indicating the ATP induced Ca^{2+} influx in RBCs (n = 25 cells from 4 repeats). Scale bar = 3 μm. (D) ExtraCal labeled, Rhod-2 AM stained, healthy human RBCs showed ExtraCal fluorescence reduction upon oxyrase addition, indicating the ATP release from RBCs due to the low O_2 tension (n = 20 cells from 4 repeats). Scale bar = 5 μm. The error bars represent SD. RBCs: Red Blood Cells; TIRF: Total Internal Reflection Fluorescence.

ganglion cells (DRGs), and white adipose tissues also demonstrated an efficient ExtraCal labeling (Figure S2). Since our primary interest in this study was to examine RBC autocrine signaling, we next examined whether human RBCs could be labeled with ExtraCal similarly. Since RBCs are nonadherent suspension cells, the optimized condition 3 with minor modifications described in Materials and Methods resulted in efficient labeling with ExtraCal.

RBC morphology has been used in previous studies as an indicator to show a correlation between cell morphology and ATP concentration using preserved blood.[43] To further confirm that the RBCs remain intact after labeling, we next examined the RBC morphologies by comparing the widefield images of labeled and unlabeled RBCs. The cell morphologies were nearly identical under both conditions, suggesting that the RBCs remained intact following the labeling process (Figure S3A,B). Additionally, we performed an absorbance scan from 450 to 800 nm to detect any peaks associated with hemoglobin in the supernatants collected by spinning ~10000 RBCs at 500 g for 2 min before and after labeling. The absence of significant differences in the absorbance spectra before and after labeling further supports that the RBCs remained intact (Figure S3C). In contrast, we observed a distinct peak corresponding to hemoglobin (540−580 nm) in the sample obtained after spinning the same number of lysed RBCs obtained by vigorously passing through a syringe with a narrow needle. Collectively, this data suggests that the cell labeling protocol preserves cell integrity.

2.2.1. Real-Time TIRF Imaging of Autocrine Regulation of ATP Release and P2X Channel-Mediated Ca^{2+} Influx in Single RBCs. Human RBCs have large replenishable stores of ATP in millimolar quantities that can be released in

https://doi.org/10.1021/cbmi.4c00067
Chem. Biomed. Imaging 2025, 3, 95−110

response to mechanical deformation, reduced pH, and exposure to decreased O_2 tension.[14,29,44] Once released into the circulation, ATP and its hydrolysis products, ADP and AMP can activate purinergic receptors and channels in the paracrine mode by acting on the vasculature,[45,46] as well as exert autocrine effects on the RBCs themselves.[47] While this paracrine signaling has been extensively investigated,[48,49] the inherent difficulties in mapping RBC signaling dynamics have led to ATP-triggered autocrine regulation of RBC function being underexplored. Though RBCs have Gq-coupled P2Y1 and P2Y2 receptors that activate PLCβ, which elevates Ca^{2+} signaling in many cells;[50] since mature RBCs do not have a sarcoplasmic reticulum, this signaling is unlikely to result in Ca^{2+} mobilization. Therefore, Ca^{2+} channels, including P2X1, P2X4, and P2X7, are likely to play a significant role in RBC Ca^{2+} homeostasis.[50] Similar to HeLa cells, we decorated the plasma membranes of healthy RBCs with the ExtraCal sensor. To avoid fluorescence interference due to hemoglobin in cells in focus and from the stratified cells in an RBC suspension while only capturing the fluorescence signals from the cells sitting on the imaging dish surface, we employed total internal reflection fluorescence (TIRF) microscopy imaging. Since our first goal was to investigate how exogenous ATP influences Ca^{2+} concentration at the cell surface, using TIRF microscopy, we examined Ca^{2+} dynamics at RBCs surfaces upon ATP addition. Considering that ATP chelates divalent cations,[51] such as Ca^{2+} and Mg^{2+}, we hypothesized that, in addition to the P2X-mediated Ca^{2+} removal due to influx, ExtraCal would also exhibit fluorescence intensity changes due to ATP-mediated Ca^{2+} chelation. ATP has an ~3-fold higher preference toward Mg^{2+} over Ca^{2+} (Mg^{2+}, K_b = 9554 ± 585 M^{-1} > Ca^{2+}, K_b = 3722 ± 211 M^{-1}).[51] Calculations show that in the presence of 5−10 mM Mg^{2+}, ATP-induced Ca^{2+} chelation is negligible. For instance, in the absence of Mg^{2+}, ~82% of Ca^{2+} is chelated by 1 μM ATP. However, in the presence of 5 mM and 10 mM Mg^{2+}, chelation reduces to ~9%, and ~5%, respectively (Figure S4). We also determined the optimum Mg^{2+} concentration needed to prevent ATP-mediated chelation of Ca^{2+}. Here, we added 100 μL of HBSS-With-Ca^{2+} into three wells in a UV transparent quartz 96-well microplate (SPECTRAplateTM). Each well was treated with 1 μL of 2 mg/mL purified GCaMP6s-LPDTG. We then treated only the second and third wells with 5 mM and 10 mM $MgCl_2$, respectively. The GCaMP6s fluorescence intensity was measured and compared before and after the 1 μM ATP addition. Compared to the well without added $MgCl_2$, GCaMP6s fluorescence reduction upon ATP addition was significantly lower in the 5 mM $MgCl_2$ treated well, while completely absent in the 10 mM $MgCl_2$ treated well (Figure 3A, one-way ANOVA: $F_{5,12}$ = 325.019, $p = 2.25 \times 10^{-12}$; Table S1A,B).

The ExtraCal labeled RBCs were resuspended at 7% hematocrit in HBSS-With-Ca^{2+} and allowed to settle for 10 min on an imaging glass-bottomed dish housed in an incubator maintained at 37 °C, 5% CO_2. Cells were then pretreated with 10 mM Mg^{2+}, and after allowing 1−2 min to reach room temperature, TIRF imaging using the Dragonfly-500 automated TIRF system was performed. We then exposed RBCs to 10 μM of ATP to activate P2X channels,[52] while continuing TIRF imaging. Upon ATP addition, RBCs exhibited an ExtraCal fluorescence loss, indicating the Ca^{2+} reduction near the RBC membranes (Figure S5A and Movie S2). Compared to the room temperature incubated cells, we also found that ATP-induced change in ExtraCal fluorescence is not influenced by the 37 °C, 5% CO_2 incubation conditions mentioned above (Figure S5B, one-way ANOVA: $F_{1,19}$ = 1.414, p = 0.25; Table S2A,B). Therefore, we conducted all the subsequent experiments under 37 °C, 5% CO_2 incubation. To further validate that the observed ExtraCal fluorescence loss is indeed due to Ca^{2+} influx, we incubated RBCs with the intracellular red Ca^{2+} sensor, Rhod-2 AM (1 μM),[53] and subsequently labeled the cells with ExtraCal. Here, we imaged a thin layer of Rhod-2 AM near the RBC membrane adjacent to the glass bottom of the dish so that the interference from the hemoglobin is averted. We controlled both the focus and the TIRF penetration depth (100 nm-120 nm) to acquire a circular area of ExtraCal fluorescence and a layer of cytosolic Rhod-2 AM signal (Figure 3B and S5C). Cells were then exposed to 10 μM of ATP to activate P2X channels. As expected, ExtraCal fluorescence reduction and Rhod-2 AM fluorescence increase were observed (Figure 3C). This indicated that the ATP induced Ca^{2+} influx (reducing extracellular Ca^{2+}) while increasing Ca^{2+} in the RBC cytosol. In a control experiment that involved the addition of only the vehicle (PBS), the cells did not exhibit a detectable ExtraCal or Rhod-2 AM fluorescence change (Figure S5D).

It has been shown that exposure to reduced O_2 tension induces ATP release from RBCs.[29,54,55] RBCs were prepared as described above and pretreated with 10 mM Mg^{2+}. We then examined whether reduced O_2 tension- induced ATP release from RBCs activates P2X channels, resulting in Ca^{2+} influx. While continuing TIRF imaging of ExtraCal and Rhod-2 AM, a reduction in O_2 tension was induced by exposing RBCs to oxyrase, an O_2 scavenger that can reduce O_2 levels down to ~3%.[29,55] Cells showed a reduction in ExtraCal fluorescence and an increase in Rhod-2 AM fluorescence intensities, indicating the P2X channel activation induced Ca^{2+} influx, likely due to low O_2-induced ATP release from RBCs (Figure 3D). RBCs labeled only with ExtraCal also showed an ~4-fold reduction in ExtraCal fluorescence upon oxyrase addition (Figure S5E and Movie S3). Next, we examined the ExtraCal fluorescence changes in labeled RBCs treated with P2X7, P2X1, or P2X4 inhibitors: A438079, NF449, or BAY1797, respectively. As expected, the RBCs exhibited a significantly lower ExtraCal fluorescence change upon the addition of oxyrase, suggesting reduced Ca^{2+} influx due to inhibition of the P2X channels (Figure S6A). This was further confirmed by a plate reader assay, in which we measured the ExtraCal fluorescence changes upon 5% oxyrase addition.

The ExtraCal fluorescence changes in inhibitor-treated labeled RBCs upon oxyrase addition were significantly lower compared to control cells (Figure S6B). In the negative control experiments in which labeled RBCs were treated with 1% PBS and unlabeled cells treated with oxyrase, the RBCs did not exhibit a significant ExtraCal fluorescence change (Figure S6B). These data collectively validated that the previously observed ExtraCal fluorescence change is due to the ATP induced-P2X channel activation and the subsequent Ca^{2+} influx.

To quantify the ATP-induced extracellular Ca^{2+} reduction due to the Ca^{2+} influx into RBCs, we determined the pre- and post-ATP concentrations of Ca^{2+} in RBC reconstituted HBSS-With-Ca^{2+}. Here, we diluted 250,000 RBCs in 1 mL of HBSS-With-Ca^{2+}, also containing 10 mM $MgCl_2$, in a 29 mm cell culture dish. To be consistent with the previous experiment, we used ExtraCal-labeled RBCs. We first removed 200 μL

https://doi.org/10.1021/cbmi.4c00067
Chem. Biomed. Imaging 2025, 3, 95−110

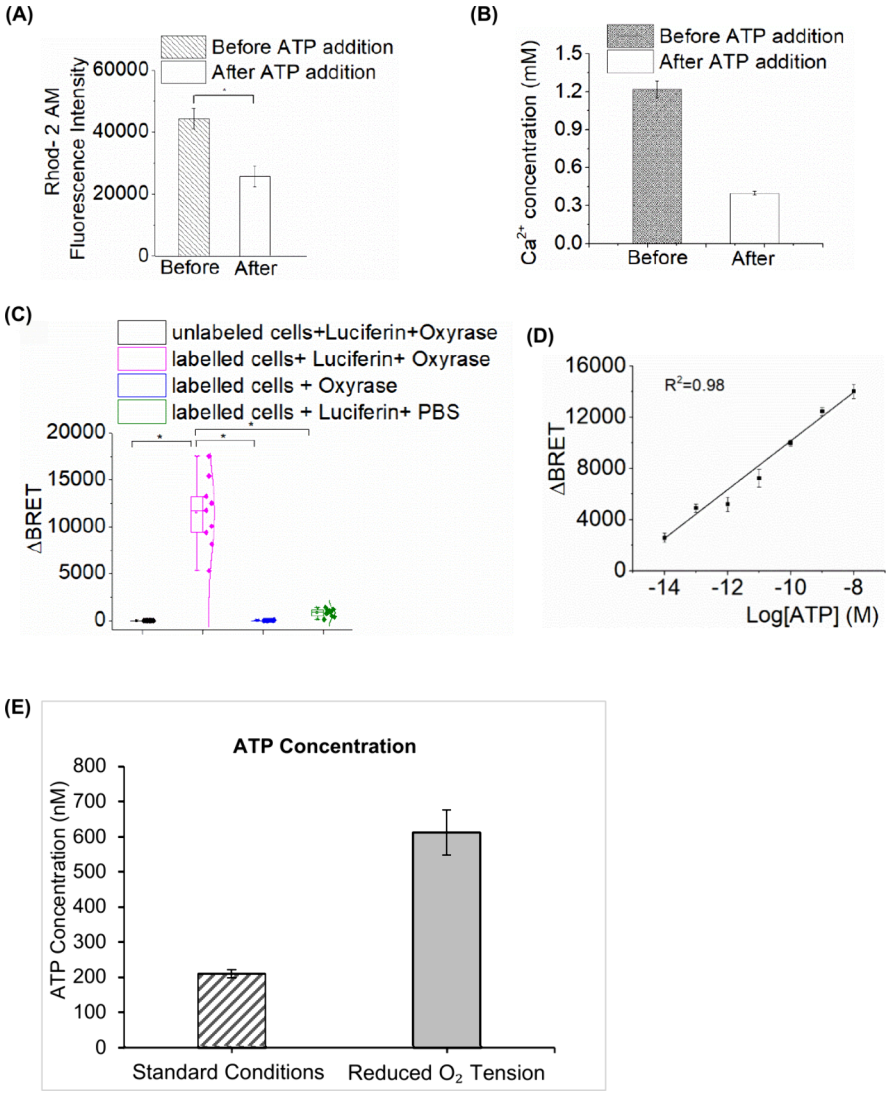

Figure 4. (A) Fluorescent plate reader assay employing Rhod-2 AM showed that extracellular media around RBCs has a lower Rhod-2 AM fluorescence intensity after ATP addition, compared to the ATP pretreated state (n = 4 replicates). (B) Fluorescent plate reader assay employing Rhod-2 AM showed that extracellular media around RBCs has a lower Ca^{2+} concentration (~0.4 mM) after ATP addition, compared to the ATP pretreated state (~1.2 mM) (n = 4 replicates). (C) luciferin treated mCherry-FLuc-labeled RBCs exhibited significant BRET gain upon oxyrase addition, compared to the RBCs in controls (n = 9 replicates from 3 days). The whisker box plot shows the observed BRET changes. (D) BRET change calibration curve obtained from a dilution series of ATP (n = 3 replicates). (E) Bar graph showing average ATP concentrations from healthy human RBCs under standard conditions and low O_2 tension (7% solution, n = 3 injections). The error bars represent SD.

aliquot of RBC media from the dish and centrifuged at 500 g at 4 °C for 2 min. This was done to remove any remaining RBCs before transferring a 100 μL aliquot of the supernatant into two wells (blank and control) of a UV transparent quartz microplate (SPECTRAplate). The control well was treated with 1 μL of Rhod-2 AM (final concentration 1 μM), while 1 μL of vehicle solvent (DMSO) was added to the blank. Similarly, the supernatants of RBCs exposed to 10 μM ATP were prepared with Rhod-2 AM. We then measured the Rhod-2 AM fluorescence intensities in these wells (Figure 4A, one-way ANOVA: $F_{1,6}$ = 44.99, $p = 5.33 \times 10^{-4}$; Table S3A,B). To calculate the corresponding Ca^{2+} concentrations from these blank-subtracted fluorescence measurements, we made a Ca^{2+} dilution series by diluting HBSS-With-Ca^{2+} in Ca^{2+}-free HBSS and similarly measured the Rhod-2 AM fluorescence intensities (Figure S6C). We verified that the manufacturer-reported Ca^{2+} concentration of HBSS (1.26 mM), is accurate by preparing a 1.26 mM $CaCl_2$ solution in Ca^{2+}-free HBSS and comparing its Rhod-2 AM fluorescence with that of HBSS-With-Ca^{2+}. A one-way ANOVA confirmed that the Ca^{2+} concentrations of both solutions were not significantly different (Figure S6D, one-way ANOVA: $F_{1,4}$ = 0.55043, p = 0.5; Table S4A,B). Collectively, our data show that the Ca^{2+} concentration of HBSS media reconstituted with RBCs before ATP is ~1.2 mM, and upon the addition of 1 μM ATP, it goes down to ~0.4 mM (Figure 4B). These data show a 3-fold reduction in the extracellular Ca^{2+} upon stimulation of RBCs with ATP.

2.2.2. Quantification of Low O_2-Induced ATP Release from RBCs. A commonly used method to detect ATP is through the chemiluminescent luciferin/luciferase reaction.[56−58] In this process, the enzyme luciferase, along with magnesium and O_2, results in a chemiluminescent reaction with ATP to result in the oxidation of the substrate luciferin.[17] This oxidation produces oxyluciferin in the excited state, which relaxes and emits light in a wavelength region between 550−570 nm.[59] To directly measure the release of ATP from RBCs

https://doi.org/10.1021/cbmi.4c00067
Chem. Biomed. Imaging 2025, 3, 95−110

under conditions of reduced extracellular O_2, we first assessed ATP on the surface of the RBCs using a bioluminescence resonance energy transfer (BRET) reaction. Subsequently, we quantified the ATP released into the surrounding media as the RBCs passed through a microfluidic channel using chemiluminescence detection.[29]

In the BRET method, we engineered a recombinant N-terminally mCherry-tethered firefly luciferase (FLuc) with a C-terminal sortase recognizing motif (mCherry-FLuc-LPDTG) in the pET32 bacterial expression vector. The aim was to enable efficient energy transfer from luciferase to mCherry upon low O_2 tension-induced ATP release from RBCs. We initially labeled the RBCs with the FLuc-BRET sensor, which is also similar to the ExtraCal labeling of RBCs. The labeled RBCs were then transferred into three sets of three wells of a white opaque 96-well tissue culture plate, with approximately 250,000 cells per well. Additionally, the same number of unlabeled RBCs was added to another set of three wells on the same plate as controls. Subsequently, 10 μL of 1 mg/mL luciferin in 1× PBS was added to the wells with unlabeled RBCs and two sets of labeled RBCs, while one set of labeled RBCs was left without luciferin. We observed the BRET signal upon the automated injection of 10 μL of oxyrase (diluted in 1× PBS to have a 5% final concentration in a well) into the wells using a plate reader. Notably, the labeled RBCs pretreated with luciferin exhibited a significant BRET gain upon oxyrase addition, indicating ATP release (Figures 4C and S7A). In comparison, no BRET change was observed in the unlabeled RBCs treated with luciferin or in the labeled RBCs without luciferin (Figure 4C). As a control, we injected 10 μL of 1× PBS instead of oxyrase into another set of wells containing luciferin-treated labeled RBCs, and these cells did not exhibit a detectable BRET change upon PBS addition (Figure 4C, one-way ANOVA: $F_{3,32} = 80.45$, $p = 5.44 \times 10^{-15}$; Table S5A, and B). Three replicates were used in each condition, and the experiments were repeated on three different days using healthy RBC samples.

To examine that extracellular ATP as the dependent variable is responsible for the observed BRET gain from FLuc-labeled RBCs, a multipoint calibration curve with ATP concentrations ranging from 10 fM to 10 nM was generated. RBCs were labeled with the FLuc- BRET sensor and prepared as above, seeded in wells of a white opaque 96-well tissue culture plate (~250,000 cells per well). We then measured the ΔBRET signal upon the addition of ATP. The resultant calibration curve exhibited a linear ΔBRET increase with the ATP concentration ($R^2 \sim 0.98$) (Figure 4D). We next converted the ΔBRET shown in Figure 4C into the amount of ATP released from RBCs. The calculations indicated that, under reduced O_2 tension, RBCs in each well released ~15 fmol of ATP. This means that each RBC released about 36,000 ATP molecules when exposed to reduced O_2 tension.

The Martin group has previously shown that a 3D-printed microfluidic device can be used to quantitate ATP release from RBCs.[29] The device (Figure S7B) introduces a 1 μL plug of RBCs into a flowing stream of buffer that mixes with a luciferin/luciferase solution (in a mixing T), and detection is accomplished via PMT. HBSS/RBC samples were pumped through the inlet of the device at 15 μL/min, and luciferin/luciferase was pumped from two syringes at a rate of 2.5 μL/min (to each side channel). The channel of the 3D-printed device mimics the physiological flow of RBCs, but with these channel dimensions and flow rates, the shear stress is less than 1 dyn/cm^2, which should not cause any shear stress-induced release of ATP in the device.[60] Quantitation was done by standard addition. In these studies, the 3D-printed device was used to quantify the concentrations of RBC-derived ATP from both RBCs under standard conditions and reduced O_2 tension (same conditions as the BRET experiments above) (Figure S7B). RBCs were separated from the whole blood of healthy volunteers, washed with PSS, diluted to 7% hematocrit, and injected into the device (standard conditions). RBC samples that have not been exposed to low O_2 tension release ATP in concentrations that vary depending on the method used and the hematocrit measured. Generally accepted values are in the hundreds of nanomolar range.[61−68] It was found that injection of RBCs (7% hematocrit) under standard conditions resulted in 210 ± 11 nM ATP (n = 3) being detected. It should be noted that values reported in this article are averages and standard deviations, with variance coming from the different injections.

It is well-documented that RBCs release ATP in response to exposure to reduced O_2 tension.[44,54,69−71] In work presented here, RBCs were also incubated with oxyrase to lower the O_2 concentration, and the RBC suspension was injected into the device.[55] It was found that these RBCs released more ATP (612 ± 64 nM, Figure 4E), and these values are consistent with those reported by Hayter et al.[29] Considering these values, the hematocrit and injection volumes, the difference between the amount of ATP released from RBCs under standard conditions and the amount released under reduced O_2 tension results in ~31,000 molecules of ATP per cell, which agrees well with the BRET measurements in the above (~36,000 ATP molecules/cell released in response to the same reduced O_2 tension conditions). Additionally, the near similar ATP releases observed by using the two experimental approaches, one using unlabeled RBCs and the other employing labeled RBCs, indicated that the RBC labeling we describe here does not significantly perturb RBC physiology.

2.3. Application of ExtraCal Sensor to Measure ATP-Induced Ca^{2+} Influx in HeLa Cells and Primary DRG Neurons

HeLa cells and dorsal root ganglion cells (DRG cells) express transcripts for most P2X and P2Y purinergic receptors.[72,73] Our in-house RNaseq data also further validate the presence of P2X1, P2X4, P2X5, P2Y1, P2Y2, P2Y6, and P2Y11 in HeLa cells (Figure S7C,D). Upon ATP addition, ATP-gated P2X channels open, and Ca^{2+} moves into the cells from the extracellular medium.[74] ATP also activates Gq-coupled P2Y receptors and hydrolyzes inner membrane phospholipid, phosphatidylinositol 4,5-bisphosphate (PIP2) into two important second messengers: diacylglycerol (DAG) and inositol 1,4,5-triphosphate (IP3).[75] IP3 then induces the mobilization of intracellular Ca^{2+}. The resulting influx and mobilization of Ca^{2+} employ a wide array of physiological effects.[76] Therefore, to examine the endogenous P2X activation in HeLa cells, we first stained cells with 1 μM Rhod-2 AM for 15 min at 37 °C as previously shown[46] and then labeled with ExtraCal according to the previously described Condition 3 protocol. Then, 1 mL of HBSS-With-Ca^{2+} was added to the cell culture dishes, and subsequently, the labeled HeLa cells were pretreated with 500 nM YM-254890, a GαqGTP inhibitor.[77,78] Then, the cells were treated with 10 mM Mg^{2+} to prevent the Ca^{2+} chelation by ATP. Finally, P2X channels were activated using 10 μM ATP. Our goal here was to inhibit P2Y receptor activation-

https://doi.org/10.1021/cbmi.4c00067
Chem. Biomed. Imaging 2025, 3, 95−110

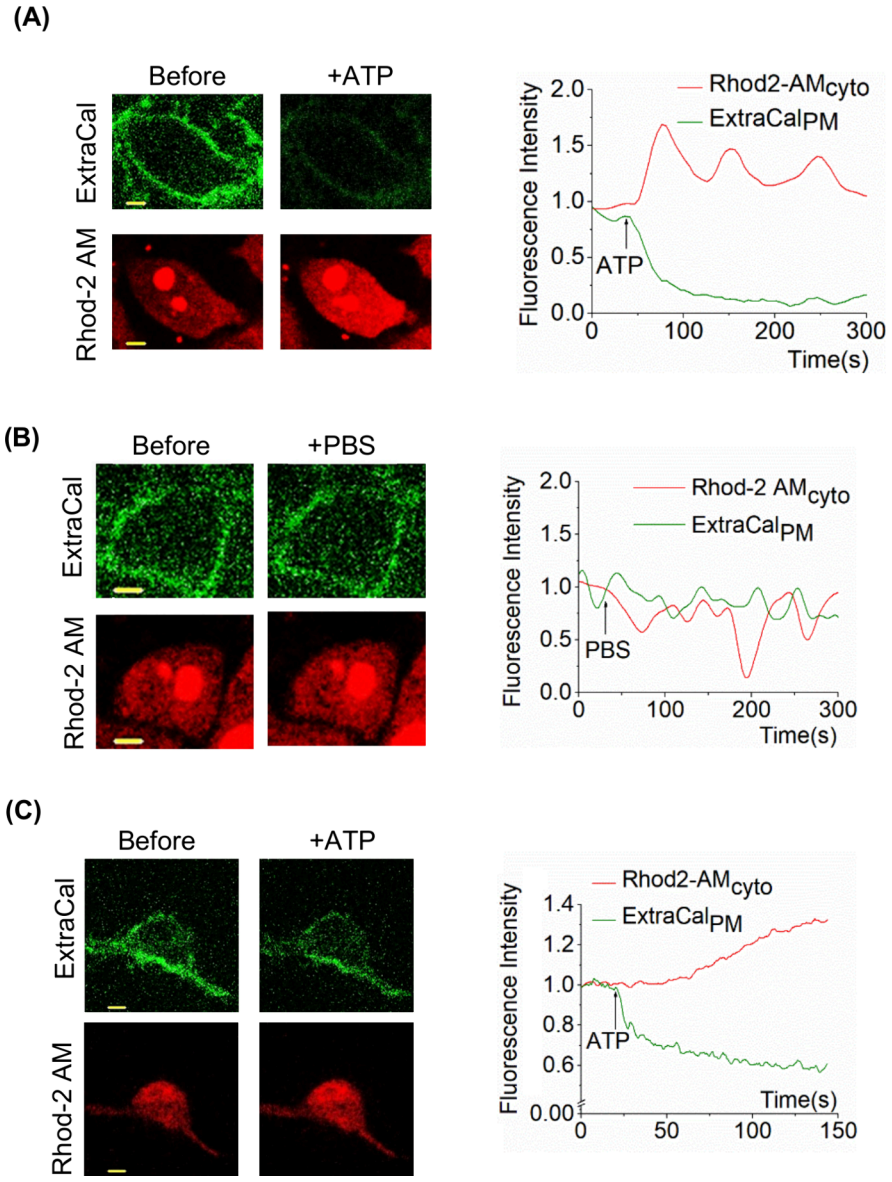

Figure 5. (A) HeLa cells labeled with ExtraCal and stained with Rhod-2 AM exhibited detectable ExtraCal fluorescence loss and Rhod-2 AM fluorescence intensity gain upon 10 μM ATP addition (n = 20 cells from 4 repeats). The plot represents fluorescence intensity changes of Rhod-2 AM and ExtraCal in response to ATP. (B) HeLa cells labeled with ExtraCal and stained with Rhod-2 AM did not show detectable ExtraCal or Rhod-2 AM fluorescence intensity changes upon PBS addition (n = 18 cells from 3 repeats). The plot shows no detectable fluorescence change with PBS. (C) Mouse dorsal root ganglion neuron cells (DRGs) labeled with ExtraCal and stained with Rhod-2 AM exhibited detectable ExtraCal fluorescence loss and Rhod-2 AM fluorescence intensity gain upon 10 μM ATP addition (n = 10 cells from 3 repeats). The plot represents the dynamic behavior of Rhod2-AM and ExtraCal in a DRG cell. Scale bar = 5 μm.

induced heterotrimer activation and PIP2 hydrolysis while only activating P2X channels. Interestingly, upon ATP addition, we observed the ExtraCal fluorescence reduction on HeLa cell membranes and Rhod-2 AM fluorescence increase in the cytosol (Figure 5A). This clearly indicated the ATP-induced P2X channel activation and the Ca^{2+} influx, which resulted in a Ca^{2+} concentration reduction in the extracellular media and an increase inside the cells. In a negative control experiment, we treated cells with the vehicle solvent (PBS), and the cells did not exhibit detectable fluorescence changes in ExtraCal or Rhod-2 AM (Figure 5B). In a positive control, we transiently transfected HeLa cells with GCaMP6s-GPI, allowing cells to present extracellularly GPI-anchored GCaMP6s at the cell surface, mimicking ExtraCal-labeled cells. We also stained these cells with Rhod 2-AM. Upon 10 μM ATP addition, similar to ExtraCal-labeled cells, cells showed GCaMP6s fluorescence loss and Rhod-2 AM fluorescence gain. This suggested that the recombinantly made ExtraCal retains a similar Ca^{2+} sensing ability (Figure S7E). We also performed a similar experiment in Rhod-2 AM stained and ExtraCal labeled mouse DRG neuron cells and observed similar responses indicating the endogenous P2X receptor activation in mouse neuron cells (Figure 5C).

3. CONCLUSION

In this study, we developed a labeling method to incorporate protein-based sensors at the cell surface in genetically intact cells. This approach utilized an engineered extracellular GCaMP6s Ca^{2+} sensor to detect Ca^{2+} dynamics at the cell surfaces, as well as a BRET sensor to detect the reduced O_2

https://doi.org/10.1021/cbmi.4c00067
Chem. Biomed. Imaging 2025, 3, 95−110

tension induced-ATP release from RBCs. We have successfully demonstrated the use of an improved sortase A (5M) enzyme, which efficiently labels the cell surfaces of various cell types (including primary cells) with high stability. This approach allows real-time monitoring of extracellular Ca^{2+} fluctuations, providing valuable insights into cellular signaling processes, such as P2X channel-mediated Ca^{2+} influx and autocrine ATP release in RBCs. Additionally, using our novel ExtraCal sensor, we have shown its ability to sense dynamic changes in extracellular Ca^{2+} under different experimental conditions. This includes exposure to EDTA, Ca^{2+} supplementation, ATP addition, and exposure to low O_2 tension. Furthermore, our application of the ExtraCal sensor in RBCs, coupled with advanced imaging techniques like TIRF microscopy, has enabled us to examine the effects of ATP on dynamic changes in extracellular and intracellular Ca^{2+} levels. This has provided a new perspective on ATP-induced Ca^{2+} signaling and its implications for cellular physiology.

The development of cell surface-localized fluorescence and BRET sensors demonstrates that these tools are versatile and effective for investigating the interplay between extracellular Ca^{2+} and ATP dynamics. Our labeling method's broad applicability across various cell types, including primary cells and RBCs, paves the way for future research into probing the dynamics and direct and indirect interactions between cell surface signaling molecules and their roles in both physiological and pathological processes.

4. MATERIALS AND METHODS

4.1. Reagents

EDTA Disodium salt dihydrate (Fisher Scientific), HBSS-With-Ca^{2+} (Gibco), Ca^{2+} free HBSS (Gibco), ATP (Chem-Impex International, Inc.)), Rhod-2 AM (Cayman Chemical), YM-254890 (Cayman Chemical), oxyrase (Oxyrase, Inc.), $MgCl_2$ hexahydrate (Sigma-Aldrich), PMSF (Research Products International), Lysozyme (Gold Biotechnology), Luciferin (Gold Biotechnology), and EZ-Run Prestained Rec Protein Ladder (Fisher Scientific). According to the manufacturer's instructions, all the reagents were dissolved in appropriate solvents and diluted in 1% Hank's balanced salt solution supplemented with $NaHCO_3$, or a regular cell culture medium, before adding to cells.

All amino acids and resins used for solid phase peptide synthesis were purchased from Chem-Impex International, Inc., as well as HOBt and piperidine. DOPE-PEG-Mal was obtained from Nanosoft Polymers. All other fine chemicals came from one of the following suppliers: Across Organics, Alpha Aesar, Ambeed, Fisher Scientific or Sigma-Aldrich. HPLC purification was achieved on a LC-20AP preparative liquid chromatograph (Shimadzu, USA) equipped with a semipreparative Viva C4 column 5 μm 150 × 10.0 mm (Restek), or on a LC-20AT analytical liquid chromatograph (Shimadzu, USA) equipped with an analytical ROC C8 5 μm 150 × 4.6 mm (Restek). MALDI-TOF data were acquired on Brüker UltrafleXtreme. MALDI samples were prepared using Super-DHB (20 mg/mL) and desalted lipopeptide solutions (1 mg/mL).

4.2. Growth and Purification of Recombinant Proteins

All expressed and purified proteins (GCaMP6-LPDTG and 5 M sortase A) were cloned into the pET32 bacterial expression vector. These constructs have Carboxy terminal His_6 tag. Sequence-verified clones were transformed into BL21(DE3) *Escherichia coli* cells. Then the cells were cultured at 37 °C overnight in 5 mL of Luria Broth (LB) media supplemented with 34 μg/mL kanamycin. This was used to inoculate 500 mL of LB media supplemented with 34 μg/mL kanamycin and cultured at 37 °C until $OD_{600} \sim 0.6$, at which point 1 mM isopropylthio-β-galactopyranoside (IPTG) was added and cultures induced overnight at 18 °C. Cells were harvested by centrifugation (4,000 rpm, 30 min, 4 °C) and the resulting pellet was resuspended in 5 mL of lysis buffer (50 mM HEPES, 300 mM NaCl, 5 mM imidazole, 10% glycerol at pH 7.2) and lysed by sonication in the presence of 100 μM PMSF and 100 μg/mL Lysozyme. To harvest the soluble fraction, the lysate was again centrifuged (11,000 rpm, 60 min, 4 °C) and the resulting supernatant was collected. Proteins of interest were isolated via Ni^{2+} affinity chromatography using HisTrap HP columns (GE) and eluted with elution buffer (50 mM HEPES, 300 mM NaCl, 250 mM imidazole, 10% glycerol at pH 7.2) using GE AKTA FPLC purifier. Protein purity was analyzed by SDS-PAGE using a 4−20% polyacrylamide gel. The protein concentration was calculated using A280 absorbance on a NanoDrop (Thermo).

4.3. SDS-PAGE Analysis and Protein Concentration Determination

Self-made polyacrylamide gels were used with self-prepared sample buffer and running buffer and stained with Coomassie Blue as described earlier.[79] Fisher BioReagents EZ-Run Prestained Rec Protein Ladder was used as the standard marker to determine the protein sizes. The protein concentrations were calculated using A280 absorbance on a NanoDrop.

4.4. Synthesis of Compounds 1 and 2

Two GPI anchor mimics were synthesized with a Gly-Gly (GG) tag at their N-terminus for sortase A coupling. Compound **1** was synthesized using the Fmoc strategy. Side chain modifications were achieved by using pseudo-orthogonal protecting group ivDde and alloc, allowing for the introduction of two palmitoyl chains, allowing the final lipopeptide to anchor in the outer leaflet of the plasma membrane, and a PEG polymer, increasing the overall solubility of the lipopeptide. Synthesis of compound **2** was achieved by mixed phase synthesis: GGGYC peptide was synthesized using Fmoc strategy then purified by HPLC before undergoing thiol-maleimide coupling with commercially available DOPE-PEG-Maleimide. Detailed syntheses and purifications of compounds **1** and **2** are available in the Supporting Information.

4.5. ExtraCal Labeling Protocol for Adherent Cells

The protocol is explained here for HeLa cells. However, the same method was used for other adherent cells by changing the respective cell culture media in place of HeLa cell culture media. In all three experimental conditions, the imaging glass-bottomed dishes with HeLa cells were first washed with 1% PBS twice and incubated with 5 μL of 10 mg/mL H_2N-GGGYC-Maleimide-PEG-DOPE (GPI anchor mimic) dissolved in 1% PBS for 10 min at 37 °C, 5% $CO_{2\ in}$ 200 μL of 1% PBS. Then the cells were washed twice with 1% PBS to remove excess unbound H_2N-GGGYC-Maleimide-PEG-DOPE.

Condition 1. After washing excess H_2N-GGGYC-Maleimide-PEG-DOPE, 100 μL of HeLa media (MEM/10% DFBS and 1% penicillin-streptomycin), 100 μL of sortase reaction buffer (500 mM Tris-HCl (pH 7.5), 1.5 M NaCl, and 100 mM $CaCl_2$), 100 μL of 2 mg/mL ExtraCal and 100 μL of 5 mg/mL sortase A (both ExtraCal and sortase A were dialyzed into 1% PBS) were mixed and added into the cell culture dish. After 10 min of incubation at 37 °C, 5% CO_2, the cell culture dishes were washed with 1% PBS twice, and 1 mL of HeLa cell culture media was added.

Condition 2. Same amounts of ExtraCal and sortase A that were dialyzed into 1% PBS were mixed with 100 μL of sortase reaction and 100 μL of 1% PBS in the cell culture dishes, in the place of HeLa cell culture media. After 10 min of incubation at 37 °C, 5% CO_2, the cell culture dishes were washed with 1% PBS twice, and 1 mL of HeLa cell culture media was added.

Condition 3. After washing excess H_2N-GGGYC-Maleimide-PEG-DOPE, 100 μL of HeLa media (MEM/10% DFBS and 1% penicillin−streptomycin), 100 μL of sortase reaction buffer, 100 μL of 2 mg/mL ExtraCal and 100 μL of 5 mg/mL sortase A (but in the elution buffer containing 300 mM NaCl, 50 mM HEPES, 10% glycerol and 250 mM imidazole) were mixed and added into the cell culture dish. After 10 min of incubation at 37 °C, 5% CO_2, the cell culture dishes were washed with 1% PBS twice, and 1 mL of HeLa cell culture media was added.

https://doi.org/10.1021/cbmi.4c00067
Chem. Biomed. Imaging 2025, 3, 95−110

4.6. Red Blood Cell Studies

The blood drawing followed a protocol approved by the Institutional Review Board of Saint Louis University. Whole blood (40 mL) was collected via venipuncture from healthy human volunteers into heparinized syringes and centrifuged at 500g and 4 °C for 10 min. The plasma and buffy coat were removed by aspiration. The remaining RBCs were washed three times with a physiological salt solution (PSS) containing 21.0 mM tris(hydroxymethyl)-aminomethane, 4.7 mM KCl, 2.0 mM $CaCl_2$, 140.5 mM NaCl, 1.2 mM $MgSO_4$, 5.5 mM glucose, and 0.5% (w/v) bovine serum albumin, at pH 7.4. RBCs were used for analysis within 2 days of drawing. When stored overnight, the RBCs were stored in PSS and washed three times the day of use. RBCs were diluted with HBSS so that the final hematocrit of the cell suspension injected into the device was 7%.

4.7. RBC Labeling Protocol

RBCs were incubated with 5 μM of H_2N-GGGYC-Maleimide-PEG-DOPE for 10 min in the incubator at 37 °C, 5% CO_2 in a closed 1.5 mL centrifuge tube. Next, the cells were centrifuged at 500*g* at 4 °C for 2 min and resuspended in 1 mL of 1% PBS. The cells were spun again (500*g* at 4 °C for 2 min) and the supernatant was removed to get rid of unbound excess H_2N-GGGYC-Maleimide-PEG-DOPE. RBCs were then resuspended in 100 μL of 1% PBS and 100 μL of sortase reaction buffer (500 mM Tris-HCl (pH 7.5), 1.5 M NaCl and 100 mM CaCl2), 100 μL of 2 mg/mL ExtraCal or mCherry-FLuc-LPDTG and 100 μL of 5 mg/mL sortase A were added. The cells were then incubated with this mixture for 10 min in the cell culture incubator under the previously described conditions in a closed 1.5 mL centrifuge tube and followed by two washing steps with 1 mL of 1% PBS.

4.8. Cell Culture

RAW264.7 and HeLa cells were purchased from ATCC, USA. Recommended cell culture media; (RAW264.7 (RPMI/10% DFBS/1% PS), and HeLa (MEM/10% DFBS/1% PS) were used to subculture cells on 29 mm, 60 mm, or 100 mm cell culture dishes. For live-cell imaging experiments, cells were seeded on 29 mm glass-bottomed dishes at a density of 1×10^5 cells/well.

4.8.1. Cell Culture and Maintenance of C2C12 and 3T3L-1 Cells. The C2C12 murine myoblasts were cultured in Dulbecco's modified Eagle growth medium (DMEM; Gibco, USA) supplemented with 10% fetal bovine serum (FBS; Gibco, USA) and 1% penicillin−streptomycin, PS (Gibco, USA). Differentiation of C2C12 cells is achieved by replacing growth media with differentiation media, DM with DMEM (Gibco), 2% horse serum (Gibco), and 1% PS (Gibco) for 7 days. The differentiation media was changed every day. The mouse 3T3-L1 preadipocytes were cultured in growth media containing 10% NB calf serum and 1% PS. When cells reached 80% confluency, the differentiation was induced by DM media with DMEM, 10% FBS, 1% PS, 500 mM IBMX,10 mM dexamethasone, and insulin (10 mg/mL) for 2 days. It was changed into DM media 2 containing DMEM, 10% FBS, 1% PS, and insulin (10 mg/mL) (Sigma-Aldrich) for the next 2 days. After 4 days of the differentiation process cells were maintained for 5 more days in standard growth media before cells were used for the experiment.

4.8.2. DRG Extraction. Matrigel was thawed on ice and diluted with cold Neurobasal medium in a ratio of 50 μL Matrigel to 1.5 mL Neurobasal. 200 μL of this mixture was added to each well of a 6-well plate with glass bottoms and incubated for 1−2 h. The mixture was gently aspirated, and the wells were allowed to dry in a hood for 3 min. Each well was washed with 500 μL Neurobasal medium and dried again in the hood. Dorsal root ganglia (DRG) were isolated from 6−8-week-old C57BL mice by anesthetizing the mice with a few drops of isoflurane in a glass container, placing the mice inside. The mice were Decapitated using large scissors, the fur was sprayed with 70% ethanol, and the dorsal skin was cut along the spinal column with medium scissors. Cuts along the sides of the spinal column were made as close to the vertebrae as possible by cutting through the arms, ribs, and hip bones while leaving some rib protrusions for orientation. The spine was placed in a large Petri dish with cold HBSSH (HBSS +HEPES) and transferred to the tissue culture room. With the help of a dissecting scope, the tissue in solution was cleaned by removing connective tissue to expose the vertebrae using small scissors. For lumbar ganglia, the last rib was cut, and then the tissue was transferred to a clean 35 mm dish with cold HBSSH. A longitudinal cut was made from the rostral to the caudal along the dorsal spinal cord using small spring scissors, and the cut was done through the bone to expose the spinal column. Using this opening as a guide, an incision was made through the ventral column with a scalpel blade, ensuring that the cut was even. From each half, the piece of spinal cord was removed carefully, avoiding pulling out the DRGs. The DRGs were plucked by inserting forceps under the DRG body to grab the distal root within the intervertebral space.

Once collected, the processes on both sides were cut with small spring scissors or a scalpel, and the DRGs samples in HBSS with 10 mM HEPES were placed on ice. The ganglia were digested in 45U papain (Worthington Biochemical) in HBSS+H for 20 min at 37 °C. After washing, the tissue was digested in collagenase (1.5 mg/mL; Sigma) for an additional 20 min at 37 °C. Following another wash, the cells were dissociated in Neurobasal A medium (Gibco) containing 5% FBS (Life Technologies), 1× B27 supplement (Gibco), 2 mM GlutaMAX (Life Technologies), and 100 U/mL penicillin/streptomycin (Life Technologies). The tissue suspension was filtered using a 40 μm nylon cell strainer and centrifuged at 1000*g* for 3 min. The cells were then resuspended, triturated, and centrifuged again at 1000*g*. Finally, the neurons were resuspended in DRG media, plated onto coverslips coated with collagen and poly-D-lysine (Sigma), and cultured for 3−4 days before proceeding with labeling and imaging experiments.

4.8.3. White Preadipose Tissue Extraction. To collect and digest adipose depots, a 1.5 mL tube for each pup was prepared, and 250 μL of phosphate-buffered saline (PBS) and 200 μL of 2× isolation buffer were added while keeping the tube with solution sterile and on ice. The P5 pups were placed into small chambers on ice until they became hypothermic, making sure that there was no direct contact with the ice. Pups were then euthanized by decapitation. For subcutaneous white adipose tissue (WAT), the pups's sides were cut and pulled down gently, and the fat depot, which appeared clear or white, was collected. For subcutaneous white adipose tissue (WAT), the pup's abdominal skin was cut and gently pulled down, and the fat depots were collected, which appeared as clear or white elongated tissue. The fat depot was rinsed in PBS and placed in a tube with PBS and isolation buffer on ice. Each depot in the tube was directly minced with small scissors. A 50 μL solution of 15 mg/mL collagenase type I in 2× isolation buffer was prepared, added to each tube and resuspended the minced tissue samples by inverting the tubes and incubating at 37 °C on a shaker for 30 min. After digestion, the tissue pieces were strained through a 100 μm cell strainer into new 50 mL tubes. These WAT suspensions were diluted enough to plate ∼4−6 wells per sample, aiming for a final volume of 2 mL per well. After 1−1.5 h, the supernatant media was aspirated, washed with 2 mL of DMEM without serum, and gently agitated to detach blood cells. After three washes, 2 mL of fresh isolation medium was added and incubated at 37 °C with 5% CO_2. The isolated WAT was maintained according to Galmozzi et al.[80] The WAT cells were also differentiated according to the 3.7.2 protocol. After 48 h (day 2 of differentiation), the medium was refreshed with a maintenance medium consisting of 10% FBS in DMEM, 1%PS, and 170 nM insulin.

4.9. Live Cell Imaging, Image Analysis, and Data Processing

The methods, protocols, and parameters for live cell imaging are adapted from previously published work.[81−83] Briefly, live cell imaging experiments were performed using a spinning disk confocal imaging system (Andor Technology) with a 60×, 1.4 NA oil objective, and iXon ULTRA 897BVback-illuminated deep-cooled EMCCD camera. The time-lapse images were analyzed using Andor iQ 3.2 software by acquiring the mean pixel fluorescence intensity changes of the entire cell or selected area/regions of interest (ROIs). Briefly, the

https://doi.org/10.1021/cbmi.4c00067
Chem. Biomed. Imaging 2025, 3, 95−110

background intensity of images was subtracted from the intensities of the ROIs assigned to the desired areas of cells (plasma membrane, and cytosol) before intensity data collection from the time-lapse images. The intensity data from multiple cells were opened in Excel (Microsoft office) and normalized to the baseline by dividing the whole data set by the average initial stable baseline value. Data were processed further using Origin-pro data analysis software (OriginLab).

4.10. Experimental Rigor and Statistical Analysis

All experiments were repeated multiple times to test the reproducibility of the results. Results are analyzed from multiple cells and represented as mean ± SD. The exact number of repeats used in the analysis is given in respective figure legends. Digital image analysis was performed using Andor iQ 3.1 software, and fluorescence intensity obtained from regions of interest was normalized to initial values (baseline). Data plot generation and statistical analysis were done using OriginPro software (OriginLab).

4.11. Cytosolic Ca^{2+} Measurements

Cells were cultured on cell culture dishes at 37 °C with 5% CO_2 for intracellular Ca^{2+} measurements. Experiments were performed 12−24 h after plating. Cells were rinsed two times with HBSS-With-Ca^{2+}, pH 7.2 and loaded with a mixture of 1 μM Rhod-2 AM (Cayman chemicals), a fluorescent probe specific for mitochondrial Ca^{2+}, with 01% Pluronic acid for 15 min at 37 °C as described previously. HBSS was removed, replaced with dye-free HeLa cell culture medium, and incubated for an additional 15 min at 37 °C. The fluorescence intensity of Rhod-2 AM was continuously imaged at 1s intervals using 594 nm excitation and 620 nm emission with confocal microscopy. Rhod-2 AM fluorescence intensities obtained from regions of interest were normalized to initial values.

4.12. Microfluidic Device

The 3D-printed device used in this study for detection of ATP from RBCs was based upon a previous design, optimized for NO and ATP detection from flowing RBCs. The device was designed in Autodesk Inventor Professional and printed on a Stratasys J750 PolyJet printer with Vero UltraClear model material. The device was manually cleaned of support material and rinsed with isopropanol and water, with small ridges that formed a carpet layer on the bottom of the device from the support material removed by wet polishing until the device was smooth and transparent. This device had some slight modifications for these studies that just focused on ATP detection.[29] All channels were designed with a 500 × 500 μm cross-section, and fluidic connections were made with printed threads design to accommodate commercial fittings (Idex P-202, IDEX Health & Science, Oak Harbor, WA) and tubing (508 mm i.d. Tygon tubing, 06419-01, Cole-Parmer) (see Figure S7B for all dimensions). The previously described device had ports for the introduction of electrodes that were not used in this study. These ports were blocked by threading various prefabricated and commercially available electrodes into the device to complete the device and possibly prevent it from leaking before ATP detection. The chemiluminescent part of the device is a significant component of this study. It consists of two inlets for introducing the luciferin/luciferase solution, followed by a straight reaction channel. The optimized design resulted in reagent streams that converge with the sample channel to form a double mixing T, and the light-producing reaction occurs as the solutions mix via diffusion in the ATP detection channel.

In this study, HBSS was used as the carrier buffer and pumped through the device at 15 μL/min from a syringe pump. Injections were made using a 4-port injector fitted with a 1 μL volume rotor (Valco Instruments, Houston, TX). The ATP/luciferin/luciferase reaction channel was placed over a PMT (Hamamatsu Photonics) in a light-excluding black box.[84] The luciferin/luciferase solution contained 10 mg/mL crude firefly lanterns (Sigma-Aldrich, St. Louis, MO), and 1 mg/mL luciferin (Gold Biotechnology, St. Louis, MO) in HBSS. The solution was sterile filtered, loaded into two syringes, and continuously pumped into the device at 2.5 μL/min. For analysis, 1 μL plugs of the standard addition samples were injected into the device. Flow injection analysis of injected RBC samples yielded peaks for chemiluminescent signal. Peak heights from ATP-spiked samples, injected in triplicate, were used to determine the concentrations of ATP in the various blood samples (standard condition vs reduced O_2 tension) via standard addition. In the range of 550−570 nm, which is the maximum emission wavelengths of the luciferin/luciferase reaction, deoxygenated hemoglobin absorbs more light than oxygenated hemoglobin.[29] Therefore, the chemiluminescent signal of ATP in reduced O_2 tension samples is attenuated relative to that in standard condition samples.[29] For this reason, separate standard curves were performed to quantitate the amount of ATP in standard conditions versus reduced O_2 tension samples. The method of standard addition was used to quantitate the ATP for all the RBC studies in order to account for any matrix effects.

All solutions were made fresh on the day of the experiment. Standard addition curves were created using 1 mL of RBCs and 0−250 μL of ATP stock solution. An ATP stock solution of 25 μM was made in HBSS. The red blood cell samples were diluted with HBSS to a final volume of 1.25 mL and a final hematocrit of 7%. RBC samples were spiked with analytes immediately before being injected into the device. Standard conditions RBCs were diluted in HBSS, whereas low O_2 conditions were achieved using oxyrase.[25,29] Reduced O_2 tension samples were diluted in HBSS with 10% oxyrase broth and incubated at room temperature for 30 min. All data, for analysis and presentation purposes, was smoothed in PeakFit (San Jose, CA) with a Savitzky−Golay filter (0.5% window) to filter the noise.

■ ASSOCIATED CONTENT

Data Availability Statement

The data sets used and analyzed during the current study are available from the corresponding author upon reasonable request.

Supporting Information

The Supporting Information is available free of charge at https://pubs.acs.org/doi/10.1021/cbmi.4c00067.

Figure S1: Validation of the Ca^{2+} sensitivity of ExtraCal; Figure S2: Wide applicability of ExtraCal labeling protocol; Figure S3: Examination of the viability of ExtraCal labeled RBCs; Figure S4: The calculations for the Ca^{2+}: ATP complex formation in the absence and presence of Mg^{2+} in the media; Figure S5: Examination of RBC autocrine signaling using ExtraCal; Figure S6: Examination of RBC autocrine signaling in P2X inhibitors treated cells. Figure S7: Relative P2X and P2Y expression in HeLa cells. Figure S8: Synthesis of target 2; Figure S9: picture of solid phase peptide synthesis apparatus; Figure S10: HPLC purification of peptide GGGYC; Figure S11: MALDI-TOF comparison of DOPE-PEG-Mal; Figure S12: Synthesis of compound 1; Figure S13: HPLC purification of compound 1; Figure S14: MALDI-TOF-TOF of compound 1; Table S1: One-way ANOVA statistics for ATP induced-Ca^{2+} chelation in HBSS-With-Calcium with and without Mg^{2+}; Table S1: One-way ANOVA statistics for ATP induced-Ca^{2+} chelation in HBSS-With-Calcium with and without Mg^{2+}; Table S2: One-way ANOVA statistics for ExtraCal fluorescence intensity changes in ExtraCal labeled RBCs settled under ambient conditions and inside the cell culture incubator, upon ATP addition; Table S3: One-way ANOVA statistics for Ca^{2+} concentrations in RBC media before and after 10 μM ATP addition (Plate reader assay); Table S4: One-way ANOVA statistics for Ca^{2+} concentrations in HBSS-With-Calcium and 1.26 mM $CaCl_2$ solution made in

https://doi.org/10.1021/cbmi.4c00067
Chem. Biomed. Imaging 2025, 3, 95−110

Calcium free HBSS; Table S5: One-way ANOVA statistics for the ΔBRET obtained upon oxyrase addition to luciferin treated-BRET sensor labeled cells and controls (PDF)
Movie S1: Ca^{2+} sensitivity of ExtraCal in HeLa cells (AVI)
Movie S2: ATP-induced P2X activation and Ca^{2+} influx in RBCs (AVI)
Movie S3: Oxyrase-induced P2X activation and Ca^{2+} influx in RBCs (AVI)

AUTHOR INFORMATION

Corresponding Authors

Steven J. Sucheck − *Department of Chemistry and Biochemistry, The University of Toledo, Toledo, Ohio 43606, United States;* orcid.org/0000-0003-0082-3827; Email: Steve.Sucheck@utoledo.edu

Ajith Karunarathne − *Department of Chemistry, Saint Louis University, Saint Louis, Missouri 63103, United States; Institute for Drug and Biotherapeutic Innovation, Saint Louis University, Saint Louis, Missouri 63103, United States;* orcid.org/0000-0003-3136-2015; Email: wkarunarathne@slu.edu

Authors

Sithurandi Ubeysinghe − *Department of Chemistry, Saint Louis University, Saint Louis, Missouri 63103, United States; Institute for Drug and Biotherapeutic Innovation, Saint Louis University, Saint Louis, Missouri 63103, United States*

Chloe O. Sebilleau − *Department of Chemistry and Biochemistry, The University of Toledo, Toledo, Ohio 43606, United States*

Waruna Thotamune − *Department of Chemistry, Saint Louis University, Saint Louis, Missouri 63103, United States; Institute for Drug and Biotherapeutic Innovation, Saint Louis University, Saint Louis, Missouri 63103, United States*

Chathuri Rajarathna − *Department of Chemistry, Saint Louis University, Saint Louis, Missouri 63103, United States; Institute for Drug and Biotherapeutic Innovation, Saint Louis University, Saint Louis, Missouri 63103, United States*

Samuel Azibere − *Department of Chemistry, Saint Louis University, Saint Louis, Missouri 63103, United States;* orcid.org/0000-0003-1302-7643

Mithila Tennakoon − *Department of Chemistry, Saint Louis University, Saint Louis, Missouri 63103, United States; Institute for Drug and Biotherapeutic Innovation, Saint Louis University, Saint Louis, Missouri 63103, United States*

John L. Payton − *College of Sciences, University of Findlay, Findlay, Ohio 45840, United States*

Randy S. Sprague − *Department of Pharmacology and Physiology, Saint Louis University School of Medicine, Saint Louis, Missouri 63104, United States*

R. Scott Martin − *Department of Chemistry, Saint Louis University, Saint Louis, Missouri 63103, United States*

Complete contact information is available at: https://pubs.acs.org/10.1021/cbmi.4c00067

Author Contributions

[§]S.U., C.O.S., and W.T. contributed equally. S.U. conducted the protein purification, cell labeling optimization and labeling, and majority of experiments; performed the data analysis; generated mCherry-FLuc BRET sensor; and performed the statistical analysis. C.O.S. synthesized the GPI anchor mimics and conducted the MALDI experiments. W.T. extracted and maintained dorsal root ganglion cells and white adipose tissues, assisted in imaging and plate reader experiments. C.R. performed protein purifications and maintained and differentiated C2C12, 3T3L, and white adipose tissues. S.A. performed RBC experiments with microfluidic devices. M.T. generated GCaMP6s-GPI and GCaMP6s-LPDTG constructs. J.L.P. performed the calculations for Ca^{2+}:ATP and Mg^{2+}:ATP complex formation. R.S.S. provided access to RBCs and reviewed the manuscript. R.S.M. reviewed the manuscript. A.K., S.U., C.O.S., W.T., C.R., S.A., and R.S.M. wrote the manuscript. A.K., S.J.S., S.U., and C.O.S. conceptualized the project.

Funding

This work was funded by NIH (NIGMS Grant R01GM140191) and Saint Louis University.

Notes

The authors declare no competing financial interest.

ACKNOWLEDGMENTS

We acknowledge Dr. Il-Man Kim (Indiana University School of Medicine, Indianapolis, IN, USA) for providing us with AC16 human cardiomyocytes. We also acknowledge Mariama Singhateh (Department of Chemistry, Saint Louis University) for assisting us with RBC processing and the Ohio Supercomputer Center for software access and computing resources.

ABBREVIATIONS

GPI glycosylphosphatidylinositol
RBC red blood cells
PIP2 phosphatidylinositol 4,5-bisphosphate
DRG dorsal root ganglion cells
EDTA ethylenediaminetetraacetic acid
HBSS Hanks' balanced salt solution
ATP adenosine triphosphate
$MgCl_2$ magnesium(II) chloride
PMSF phenylmethylsulfonyl fluoride
TIRF total internal reflection fluorescence
PMT photomultiplier tube

REFERENCES

(1) Patergnani, S.; Suski, J. M.; Agnoletto, C.; Bononi, A.; Bonora, M.; De Marchi, E.; Giorgi, C.; Marchi, S.; Missiroli, S.; Poletti, F.; et al. Calcium signaling around Mitochondria Associated Membranes (MAMs). *Cell Commun. Signaling* **2011**, *9* (1), 19.
(2) Thul, R.; Coombes, S.; Roderick, H. L.; Bootman, M. D. Subcellular calcium dynamics in a whole-cell model of an atrial myocyte. *Proc. Natl. Acad. Sci. U. S. A.* **2012**, *109* (6), 2150−2155.
(3) Calaghan, S. C.; White, E. The role of calcium in the response of cardiac muscle to stretch. *Prog. Biophys. Mol. Biol.* **1999**, *71* (1), 59−90.
(4) Bagur, R.; Hajnoczky, G. Intracellular Ca^{2+} Sensing: Its Role in Calcium Homeostasis and Signaling. *Mol. Cell* **2017**, *66* (6), 780−788.
(5) Sinha, S.; Elbaz-Alon, Y.; Avinoam, O. Ca^{2+} as a coordinator of skeletal muscle differentiation, fusion and contraction. *FEBS J.* **2022**, *289* (21), 6531−6542.
(6) Stafford, N.; Wilson, C.; Oceandy, D.; Neyses, L.; Cartwright, E. J. The Plasma Membrane Calcium ATPases and Their Role as Major New Players in Human Disease. *Physiol. Rev.* **2017**, *97* (3), 1089−1125.

(7) Cerella, C.; Diederich, M.; Ghibelli, L. The dual role of calcium as messenger and stressor in cell damage, death, and survival. *Int. J. Cell Biol.* **2010**, *2010* (1), No. 546163.
(8) Atchison, D. K.; Beierwaltes, W. H. The influence of extracellular and intracellular calcium on the secretion of renin. *Pflugers Arch.* **2013**, *465* (1), 59−69.
(9) Nicholson, C.; Bruggencate, G. T.; Steinberg, R.; Stockle, H. Calcium modulation in brain extracellular microenvironment demonstrated with ion-selective micropipette. *Proc. Natl. Acad. Sci. U. S. A.* **1977**, *74* (3), 1287−1290.
(10) Mupanomunda, M. M.; Tian, B.; Ishioka, N.; Bukoski, R. D. Renal interstitial Ca^{2+}. *Am. J. Physiol.: Renal Physiol.* **2000**, *278* (4), F644−649.
(11) Gerbino, A.; Colella, M. The Different Facets of Extracellular Calcium Sensors: Old and New Concepts in Calcium-Sensing Receptor Signalling and Pharmacology. *Int. J. Mol. Sci.* **2018**, *19* (4), No. 999.
(12) Cilek, N.; Ugurel, E.; Goksel, E.; Yalcin, O. Signaling mechanisms in red blood cells: A view through the protein phosphorylation and deformability. *J. Cell Physiol.* **2024**, *239* (3), No. e30958.
(13) van Dijk, M. J.; de Wilde, J. R. A.; Bartels, M.; Kuo, K. H. M.; Glenthoj, A.; Rab, M. A. E.; van Beers, E. J.; van Wijk, R. Activation of pyruvate kinase as therapeutic option for rare hemolytic anemias: Shedding new light on an old enzyme. *Blood Rev.* **2023**, *61*, 101103.
(14) Olearczyk, J. J.; Stephenson, A. H.; Lonigro, A. J.; Sprague, R. S. Receptor-mediated activation of the heterotrimeric G-protein Gs results in ATP release from erythrocytes. *Med. Sci. Monit.* **2001**, *7* (4), 669−674.
(15) Olearczyk, J. J.; Stephenson, A. H.; Lonigro, A. J.; Sprague, R. S. Heterotrimeric G protein Gi is involved in a signal transduction pathway for ATP release from erythrocytes. *Am. J. Physiol.: Heart Circ. Physiol.* **2004**, *286* (3), H940−945.
(16) Sprague, R.; Stephenson, A.; Bowles, E.; Stumpf, M.; Ricketts, G.; Lonigro, A. Expression of the heterotrimeric G protein Gi and ATP release are impaired in erythrocytes of humans with diabetes mellitus. *Adv. Exp. Med. Biol.* **2006**, *588*, 207−216.
(17) Sprague, R. S.; Bowles, E. A.; Hanson, M. S.; DuFaux, E. A.; Sridharan, M.; Adderley, S.; Ellsworth, M. L.; Stephenson, A. H. Prostacyclin analogs stimulate receptor-mediated cAMP synthesis and ATP release from rabbit and human erythrocytes. *Microcirculation* **2008**, *15* (5), 461−471.
(18) Bogdanova, A.; Makhro, A.; Wang, J.; Lipp, P.; Kaestner, L. Calcium in red blood cells-a perilous balance. *Int. J. Mol. Sci.* **2013**, *14* (5), 9848−9872.
(19) Kuck, L.; Peart, J. N.; Simmonds, M. J. Calcium dynamically alters erythrocyte mechanical response to shear. *Biochim. Biophys. Acta, Mol. Cell Res.* **2020**, *1867* (11), 118802.
(20) D'Amici, G. M.; Rinalducci, S.; Zolla, L. Proteomic analysis of RBC membrane protein degradation during blood storage. *J. Proteome Res.* **2007**, *6* (8), 3242−3255.
(21) Dybas, J.; Alcicek, F. C.; Wajda, A.; Kaczmarska, M.; Zimna, A.; Bulat, K.; Blat, A.; Stepanenko, T.; Mohaissen, T.; Szczesny-Malysiak, E.; et al. Trends in biomedical analysis of red blood cells - Raman spectroscopy against other spectroscopic, microscopic and classical techniques. *TrAC, Trends Anal. Chem.* **2022**, *146*, No. 116481.
(22) Barasa, B.; Slijper, M. Challenges for red blood cell biomarker discovery through proteomics. *Biochim. Biophys. Acta* **2014**, *1844* (5), 1003−1010.
(23) Grigorev, G. V.; Lebedev, A. V.; Wang, X.; Qian, X.; Maksimov, G. V.; Lin, L. Advances in Microfluidics for Single Red Blood Cell Analysis. *Biosensors (Basel)* **2023**, *13* (1), No. 117.
(24) Sprague, R. S.; Ellsworth, M. L. Erythrocyte-derived ATP and perfusion distribution: role of intracellular and intercellular communication. *Microcirculation* **2012**, *19* (5), 430−439.
(25) Edwards, J.; Sprung, R.; Sprague, R.; Spence, D. Chemiluminescence detection of ATP release from red blood cells upon passage through microbore tubing. *Analyst* **2001**, *126* (8), 1257−1260.
(26) Price, A. K.; Fischer, D. J.; Martin, R. S.; Spence, D. M. Deformation-induced release of ATP from erythrocytes in a poly(dimethylsiloxane)-based microchip with channels that mimic resistance vessels. *Anal. Chem.* **2004**, *76* (16), 4849−4855.
(27) Sprung, R.; Sprague, R.; Spence, D. Determination of ATP release from erythrocytes using microbore tubing as a model of resistance vessels in vivo. *Anal. Chem.* **2002**, *74* (10), 2274−2278.
(28) Townsend, A. D.; Sprague, R. S.; Martin, R. S. Microfluidic device using a gold pillar array and integrated electrodes for on-chip endothelial cell immobilization, direct RBC contact, and amperometric detection of nitric oxide. *Electroanalysis* **2019**, *31* (8), 1409−1415.
(29) Hayter, E. A.; Azibere, S.; Skrajewski, L. A.; Soule, L. D.; Spence, D. M.; Martin, R. S. A 3D-printed, multi-modal microfluidic device for measuring nitric oxide and ATP release from flowing red blood cells. *Anal. Methods* **2022**, *14* (33), 3171−3179.
(30) Simitian, G.; Virumbrales-Munoz, M.; Sanchez-de-Diego, C.; Beebe, D. J.; Kosoff, D. Microfluidics in vascular biology research: a critical review for engineers, biologists, and clinicians. *Lab Chip* **2022**, *22* (19), 3618−3636.
(31) Jenkins, M.; Ratnaike, S. Capillary electrophoresis of hemoglobin. *Clin. Chem. Lab Med.* **2003**, *41* (6), 747−754.
(32) Pretini, V.; Koenen, M. H.; Kaestner, L.; Fens, M.; Schiffelers, R. M.; Bartels, M.; Van Wijk, R. Red Blood Cells: Chasing Interactions. *Front. Physiol.* **2019**, *10*, No. 945.
(33) Kinoshita, T. Glycosylphosphatidylinositol (GPI) Anchors: Biochemistry and Cell Biology: Introduction to a Thematic Review Series. *J. Lipid Res.* **2016**, *57* (1), 4−5.
(34) Kinoshita, T. Biosynthesis and biology of mammalian GPI-anchored proteins. *Open Biol.* **2020**, *10* (3), No. 190290.
(35) Kinoshita, T.; Fujita, M. Biosynthesis of GPI-anchored proteins: special emphasis on GPI lipid remodeling. *J. Lipid Res.* **2016**, *57* (1), 6−24.
(36) Olschewski, D.; Seidel, R.; Miesbauer, M.; Rambold, A. S.; Oesterhelt, D.; Winklhofer, K. F.; Tatzelt, J.; Engelhard, M.; Becker, C. F. Semisynthetic murine prion protein equipped with a GPI anchor mimic incorporates into cellular membranes. *Chem. Biol.* **2007**, *14* (9), 994−1006.
(37) Guo, Z. Synthetic Studies of Glycosylphosphatidylinositol (GPI) Anchors and GPI-Anchored Peptides, Glycopeptides, and Proteins. *Curr. Org. Synth* **2013**, *10* (3), 366−383.
(38) Theile, C. S.; Witte, M. D.; Blom, A. E.; Kundrat, L.; Ploegh, H. L.; Guimaraes, C. P. Site-specific N-terminal labeling of proteins using sortase-mediated reactions. *Nat. Protoc.* **2013**, *8* (9), 1800−1807.
(39) Tomita, U.; Yamaguchi, S.; Maeda, Y.; Chujo, K.; Minamihata, K.; Nagamune, T. Protein cell-surface display through in situ enzymatic modification of proteins with a poly(Ethylene glycol)-lipid. *Biotechnol. Bioeng.* **2013**, *110* (10), 2785−2789.
(40) Chen, T. W.; Wardill, T. J.; Sun, Y.; Pulver, S. R.; Renninger, S. L.; Baohan, A.; Schreiter, E. R.; Kerr, R. A.; Orger, M. B.; Jayaraman, V.; et al. Ultrasensitive fluorescent proteins for imaging neuronal activity. *Nature* **2013**, *499* (7458), 295−300.
(41) Chen, I.; Dorr, B. M.; Liu, D. R. A general strategy for the evolution of bond-forming enzymes using yeast display. *Proc. Natl. Acad. Sci. U. S. A.* **2011**, *108* (28), 11399−11404.
(42) Jeong, H. J.; Abhiraman, G. C.; Story, C. M.; Ingram, J. R.; Dougan, S. K. Generation of Ca^{2+}-independent sortase A mutants with enhanced activity for protein and cell surface labeling. *PLoS One* **2017**, *12* (12), No. e0189068.
(43) Leonart, M. S.; Nascimento, A. J.; Nonoyama, K.; Pelissari, C. B.; Stinghen, A. E.; Barretto, O. C. Correlation of discocyte frequency and ATP concentration in preserved blood. A morphological indicator of red blood cell viability. *Braz. J. Med. Biol. Res.* **1997**, *30* (6), 745−747.
(44) Ellsworth, M. L.; Ellis, C. G.; Goldman, D.; Stephenson, A. H.; Dietrich, H. H.; Sprague, R. S. Erythrocytes: oxygen sensors and modulators of vascular tone. *Physiology (Bethesda)* **2009**, *24*, 107−116.

https://doi.org/10.1021/cbmi.4c00067
Chem. Biomed. Imaging 2025, 3, 95−110

(45) Nayak, A. K.; Das, S. L.; Misbah, C. Endothelial calcium dynamics elicited by ATP release from red blood cells. *Sci. Rep.* **2024**, *14* (1), No. 13550.
(46) Rhett, J. M.; Fann, S. A.; Yost, M. J. Purinergic signaling in early inflammatory events of the foreign body response: modulating extracellular ATP as an enabling technology for engineered implants and tissues. *Tissue Eng., Part B* **2014**, *20* (5), 392−402.
(47) Sabirov, R. Z.; Okada, Y. ATP-conducting maxi-anion channel: a new player in stress-sensory transduction. *Jpn. J. Physiol.* **2004**, *54* (1), 7−14.
(48) Wei, L.; Mousawi, F.; Li, D.; Roger, S.; Li, J.; Yang, X.; Jiang, L. H. Adenosine Triphosphate Release and P2 Receptor Signaling in Piezo1 Channel-Dependent Mechanoregulation. *Front. Pharmacol.* **2019**, *10*, No. 1304.
(49) Corriden, R.; Insel, P. A. Basal release of ATP: an autocrine-paracrine mechanism for cell regulation. *Sci. Signaling* **2010**, *3* (104), re1.
(50) Sluyter, R. P2X and P2Y receptor signaling in red blood cells. *Front Mol. Biosci* **2015**, *2*, No. 60.
(51) Wilson, J. E.; Chin, A. Chelation of divalent cations by ATP, studied by titration calorimetry. *Anal. Biochem.* **1991**, *193* (1), 16−19.
(52) Illes, P.; Muller, C. E.; Jacobson, K. A.; Grutter, T.; Nicke, A.; Fountain, S. J.; Kennedy, C.; Schmalzing, G.; Jarvis, M. F.; Stojilkovic, S. S.; et al. Update of P2X receptor properties and their pharmacology: IUPHAR Review 30. *Br. J. Pharmacol.* **2021**, *178* (3), 489−514.
(53) Elamin, E.; Masclee, A.; Troost, F.; Dekker, J.; Jonkers, D. Cytotoxicity and metabolic stress induced by acetaldehyde in human intestinal LS174T goblet-like cells. *Am. J. Physiol.: Gastrointest. Liver Physiol.* **2014**, *307* (3), G286−G294.
(54) Bergfeld, G. R.; Forrester, T. Release of ATP from human erythrocytes in response to a brief period of hypoxia and hypercapnia. *Cardiovasc. Res.* **1992**, *26* (1), 40−47.
(55) Halpin, S. T.; Spence, D. M. Direct plate-reader measurement of nitric oxide released from hypoxic erythrocytes flowing through a microfluidic device. *Anal. Chem.* **2010**, *82* (17), 7492−7497.
(56) Racine, M. L.; Dinenno, F. A. Reduced deformability contributes to impaired deoxygenation-induced ATP release from red blood cells of older adult humans. *J. Physiol.* **2019**, *597* (17), 4503−4519.
(57) Kirby, B. S.; Sparks, M. A.; Lazarowski, E. R.; Lopez Domowicz, D. A.; Zhu, H.; McMahon, T. J. Pannexin 1 channels control the hemodynamic response to hypoxia by regulating O(2)-sensitive extracellular ATP in blood. *Am. J. Physiol.: Heart Circ. Physiol.* **2021**, *320* (3), H1055−H1065.
(58) Sikora, J.; Orlov, S. N.; Furuya, K.; Grygorczyk, R. Hemolysis is a primary ATP-release mechanism in human erythrocytes. *Blood* **2014**, *124* (13), 2150−2157.
(59) Marques, S. M.; Esteves da Silva, J. C. Firefly bioluminescence: a mechanistic approach of luciferase catalyzed reactions. *IUBMB Life* **2009**, *61* (1), 6−17.
(60) Papaioannou, T. G.; Stefanadis, C. Vascular wall shear stress: basic principles and methods. *Hellenic J. Cardiol.* **2005**, *46* (1), 9−15.
(61) Castiaux, A. D.; Pinger, C. W.; Hayter, E. A.; Bunn, M. E.; Martin, R. S.; Spence, D. M. PolyJet 3D-Printed Enclosed Microfluidic Channels without Photocurable Supports. *Anal. Chem.* **2019**, *91* (10), 6910−6917.
(62) Nishiyama, K.; Mizukami, R.; Kuki, S.; Ishida, A.; Chida, J.; Kido, H.; Maeki, M.; Tani, H.; Tokeshi, M. Electrochemical enzyme-based blood ATP and lactate sensor for a rapid and straightforward evaluation of illness severity. *Biosens. Bioelectron.* **2022**, *198*, 113832.
(63) Price, A. K.; Martin, R. S.; Spence, D. M. Monitoring erythrocytes in a microchip channel that narrows uniformly: towards an improved microfluidic-based mimic of the microcirculation. *J. Chromatogr. A* **2006**, *1111* (2), 220−227.
(64) Cinar, E.; Zhou, S.; DeCourcey, J.; Wang, Y.; Waugh, R. E.; Wan, J. Piezo1 regulates mechanotransductive release of ATP from human RBCs. *Proc. Natl. Acad. Sci. U. S. A.* **2015**, *112* (38), 11783−11788.
(65) Moehlenbrock, M. J.; Price, A. K.; Martin, R. S. Use of microchip-based hydrodynamic focusing to measure the deformation-induced release of ATP from erythrocytes. *Analyst* **2006**, *131* (8), 930−937.
(66) Wan, J.; Ristenpart, W. D.; Stone, H. A. Dynamics of shear-induced ATP release from red blood cells. *Proc. Natl. Acad. Sci. U. S. A.* **2008**, *105* (43), 16432−16437.
(67) Carroll, J. S.; Ku, C. J.; Karunarathne, W.; Spence, D. M. Red blood cell stimulation of platelet nitric oxide production indicated by quantitative monitoring of the communication between cells in the bloodstream. *Anal. Chem.* **2007**, *79* (14), 5133−5138.
(68) Mortensen, S. P.; Thaning, P.; Nyberg, M.; Saltin, B.; Hellsten, Y. Local release of ATP into the arterial inflow and venous drainage of human skeletal muscle: insight from ATP determination with the intravascular microdialysis technique. *J. Physiol.* **2011**, *589* (7), 1847−1857.
(69) Cosby, K.; Partovi, K. S.; Crawford, J. H.; Patel, R. P.; Reiter, C. D.; Martyr, S.; Yang, B. K.; Waclawiw, M. A.; Zalos, G.; Xu, X.; et al. Nitrite reduction to nitric oxide by deoxyhemoglobin vasodilates the human circulation. *Nat. Med.* **2003**, *9* (12), 1498−1505.
(70) Nagababu, E.; Ramasamy, S.; Abernethy, D. R.; Rifkind, J. M. Active nitric oxide produced in the red cell under hypoxic conditions by deoxyhemoglobin-mediated nitrite reduction. *J. Biol. Chem.* **2003**, *278* (47), 46349−46356.
(71) Webb, A. J.; Milsom, A. B.; Rathod, K. S.; Chu, W. L.; Qureshi, S.; Lovell, M. J.; Lecomte, F. M.; Perrett, D.; Raimondo, C.; Khoshbin, E.; et al. Mechanisms underlying erythrocyte and endothelial nitrite reduction to nitric oxide in hypoxia: role for xanthine oxidoreductase and endothelial nitric oxide synthase. *Circ. Res.* **2008**, *103* (9), 957−964.
(72) Welter-Stahl, L.; da Silva, C. M.; Schachter, J.; Persechini, P. M.; Souza, H. S.; Ojcius, D. M.; Coutinho-Silva, R. Expression of purinergic receptors and modulation of P2X7 function by the inflammatory cytokine IFNγ in human epithelial cells. *Biochim. Biophys. Acta* **2009**, *1788* (5), 1176−1187.
(73) Burgard, E. C.; Niforatos, W.; van Biesen, T.; Lynch, K. J.; Touma, E.; Metzger, R. E.; Kowaluk, E. A.; Jarvis, M. F. P2X receptor-mediated ionic currents in dorsal root ganglion neurons. *J. Neurophysiol.* **1999**, *82* (3), 1590−1598.
(74) Samways, D. S.; Li, Z.; Egan, T. M. Principles and properties of ion flow in P2X receptors. *Front. Cell Neurosci.* **2014**, *8*, No. 6.
(75) Van Kolen, K.; Slegers, H. Integration of P2Y receptor-activated signal transduction pathways in G protein-dependent signalling networks. *Purinergic Signaling* **2006**, *2* (3), 451−469.
(76) Puchalowicz, K.; Tarnowski, M.; Baranowska-Bosiacka, I.; Chlubek, D.; Dziedziejko, V. P2X and P2Y receptors-role in the pathophysiology of the nervous system. *Int. J. Mol. Sci.* **2014**, *15* (12), 23672−23704.
(77) Tietze, D.; Kaufmann, D.; Tietze, A. A.; Voll, A.; Reher, R.; Konig, G.; Hausch, F. Structural and Dynamical Basis of G Protein Inhibition by YM-254890 and FR900359: An Inhibitor in Action. *J. Chem. Inf. Model.* **2019**, *59* (10), 4361−4373.
(78) Ubeysinghe, S.; Kankanamge, D.; Thotamune, W.; Wijayaratna, D.; Mohan, T. M., 3rd; Karunarathne, A. Spatiotemporal Optical Control of Galphaq-PLCbeta Interactions. *ACS Synth. Biol.* **2024**, *13* (1), 242−258.
(79) Mazur, P.; Dumnicka, P.; Tisonczyk, J.; Zabek-Adamska, A.; Drozdz, R. SDS Electrophoresis on Gradient Polyacrylamide Gels as a Semiquantitative Tool for the Evaluation of Proteinuria. *Diagnostics (Basel)* **2023**, *13* (9), No. 1513.
(80) Galmozzi, A.; Kok, B. P.; Saez, E. Isolation and Differentiation of Primary White and Brown Preadipocytes from Newborn Mice. *J. Vis Exp* **2021**, No. 167, No. e62005.
(81) Ratnayake, K.; Payton, J. L.; Lakmal, O. H.; Karunarathne, A. Blue light excited retinal intercepts cellular signaling. *Sci. Rep* **2018**, *8* (1), No. 10207.
(82) Ratnayake, K.; Payton, J. L.; Meger, M. E.; Godage, N. H.; Gionfriddo, E.; Karunarathne, A. Blue light-triggered photochemistry and cytotoxicity of retinal. *Cell Signaling* **2020**, *69*, No. 109547.

https://doi.org/10.1021/cbmi.4c00067
Chem. Biomed. Imaging 2025, 3, 95−110

(83) Senarath, K.; Ratnayake, K.; Siripurapu, P.; Payton, J. L.; Karunarathne, A. Reversible G Protein betagamma9 Distribution-Based Assay Reveals Molecular Underpinnings in Subcellular, Single-Cell, and Multicellular GPCR and G Protein Activity. *Anal. Chem.* **2016**, *88* (23), 11450−11459.
(84) Hayter, E. A.; Castiaux, A. D.; Martin, R. S. 3D-Printed Microfluidic Device with In-line Amperometric Detection that Also Enables Multi-Modal Detection. *Anal. Methods* **2020**, *12* (15), 2046−2051.

https://doi.org/10.1021/cbmi.4c00067
Chem. Biomed. Imaging 2025, 3, 95−110